ALPs and X-ray astronomy

Kuver Sinha
University of Oklahoma

Based on arXiv:1804.01992, arXiv:1807.10773
with Jean-Francois Fortin

astrophysics: Matthew Baring (Rice University), Eddie Baron (Oklahoma),
Henric Krawczynski (WUSTL), Mark Alford (WUSTL)

Introduction

ALPs: strong CP problem, string axiverse, etc.

Detection typically relies on ALP couplings:

$$\mathcal{L} \supset -\frac{g}{4} a F_{\mu\nu} \tilde{F}^{\mu\nu} + g_{aN} (\partial_\mu a) \bar{N} \gamma^\mu \gamma_5 N$$

Strong magnetic fields are especially useful

Neutron stars have the strongest magnetic fields

Also lots of data

Helioscope

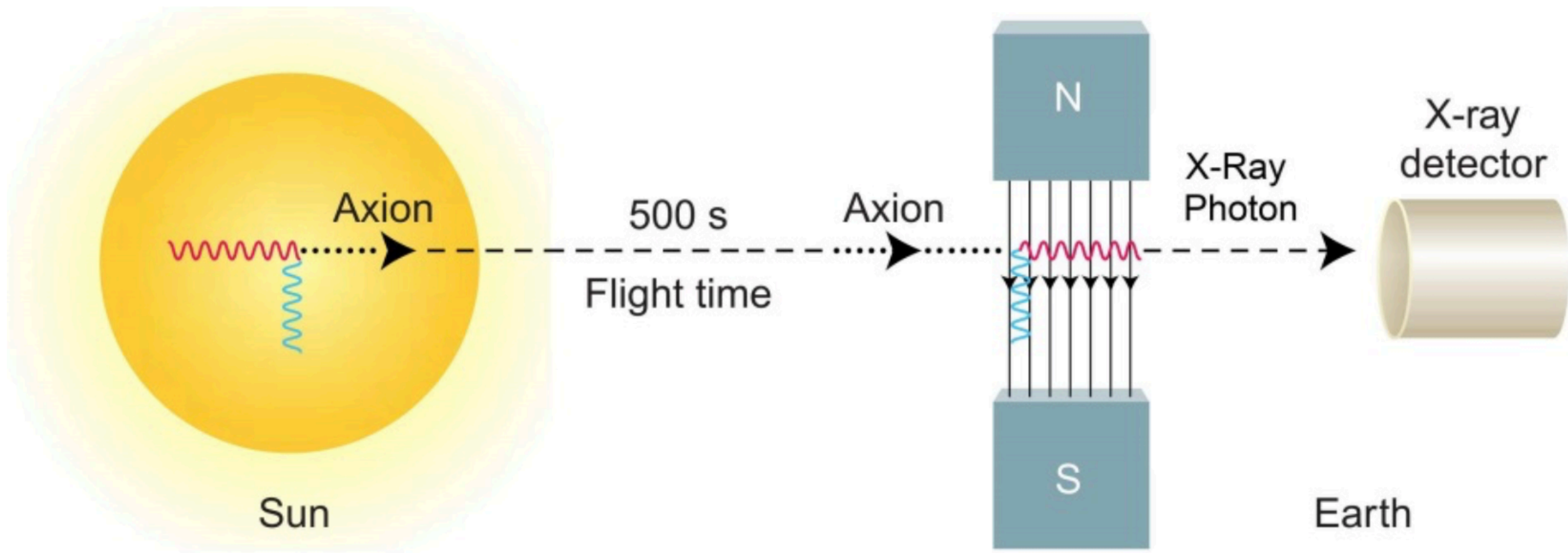

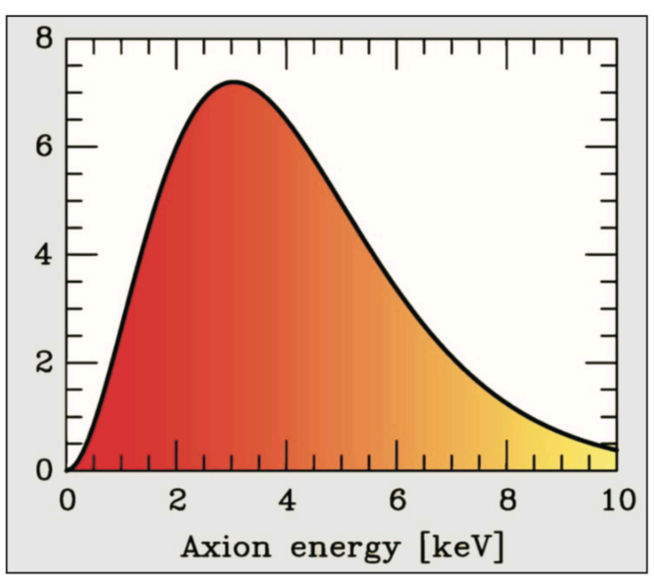

$$\mathcal{L} \supset -\frac{g}{4} a F_{\mu\nu} \tilde{F}^{\mu\nu}$$

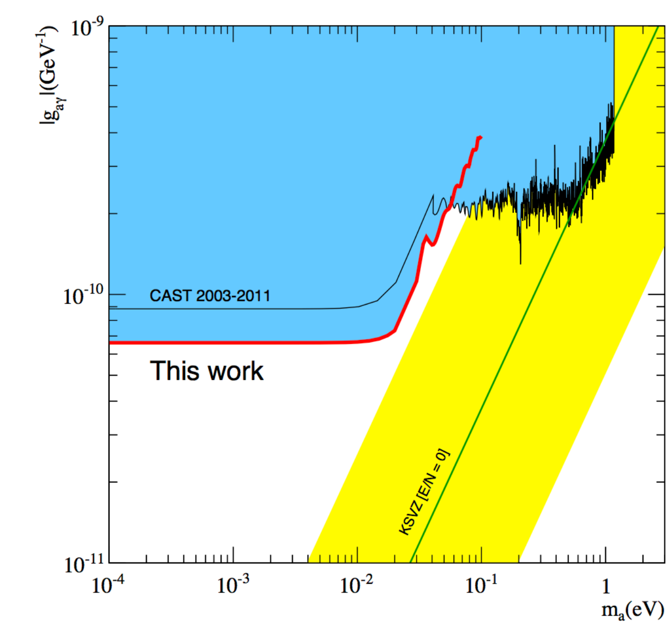

CAST (2017)

Main Idea

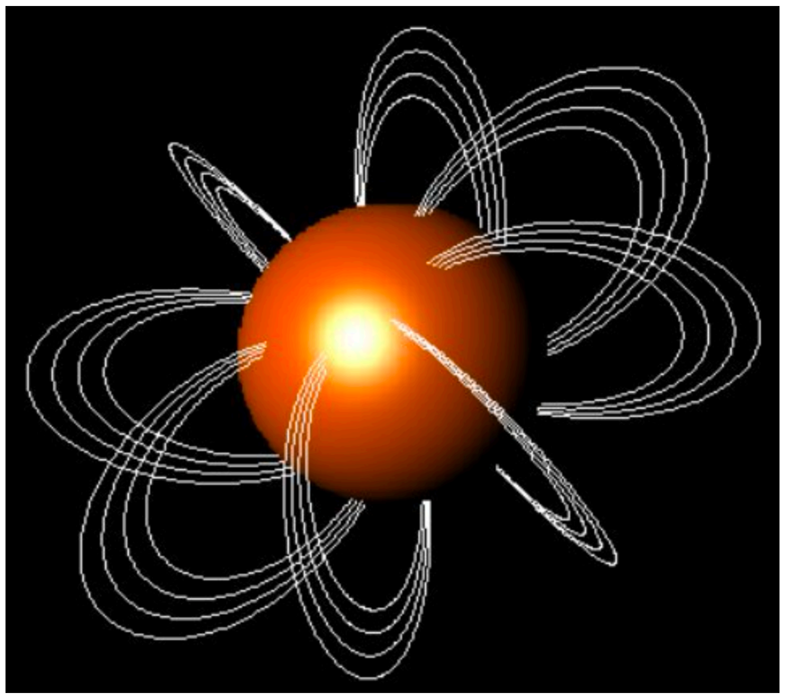

$$B_0 = 20 \times 10^{14}\,\mathrm{G}$$

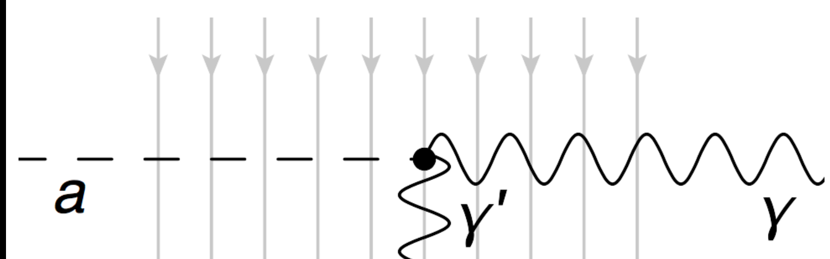

$$B = B_0 (r_0/r)^3$$

Hard X-rays

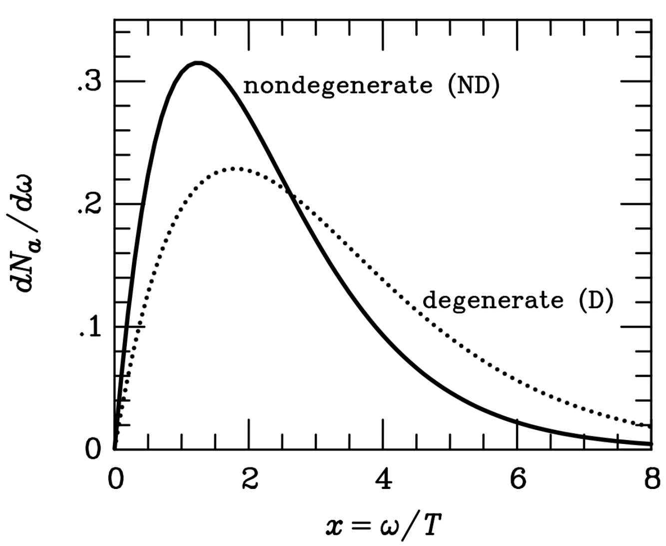

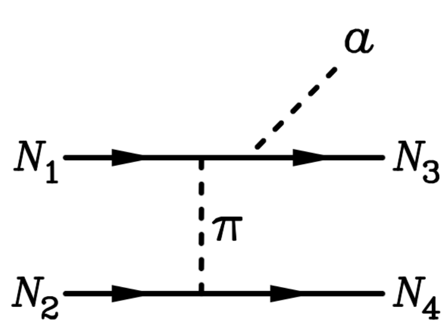

Soft X-rays

Heyl/Lai (2006)

Perna et. al. (2012)

Radio Waves

Pshirkov/Popov (2007)

Hook/Kahn/Safdi (2018)

Probability
of
Conversion

ALP Wave Equation

$\mathbf{E}, a \propto e^{i\omega t}$

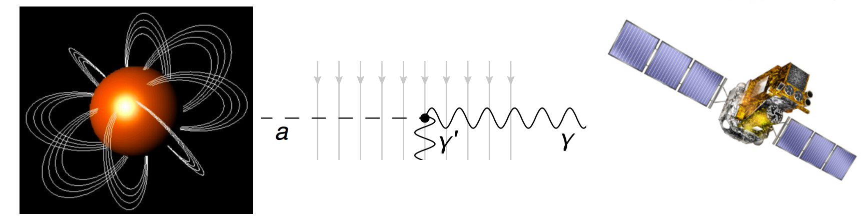

photon wavelength much smaller than magnetar radius

linearized wave equation

$$i\frac{d}{dr}\begin{pmatrix} a \\ E_{\parallel} \end{pmatrix} = \begin{pmatrix} \omega + \Delta_a & \Delta_M \\ \Delta_M & \omega + \Delta_{\parallel} \end{pmatrix} \begin{pmatrix} a \\ E_{\parallel} \end{pmatrix}$$

Raffelt/Stodolsky (1988)

axion mass term $\Delta_a = -\frac{m_a^2}{2\omega}$

mixing term $\Delta_M = \frac{1}{2} g B \sin\theta$

Euler-Heisenberg term $\Delta_{\parallel} = \frac{1}{2} q \omega \sin^2\theta$ $\quad q = \frac{7\alpha}{45\pi} b^2 \hat{q}$ $\quad \hat{q} = \frac{1 + 1.2b}{1 + 1.33b + 0.56b^2}$

Schwinger (1951), Adler (1971), Heyl/Hernquist (2010)

magnetic field $b = B/B_Q$

$$B_Q = m_e^2 c^3/(e\hbar) = 4.414 \times 10^{13}\ \mathrm{G}$$

Mixing Angle

$$i\frac{d}{dx}\begin{pmatrix} a \\ E_\parallel \end{pmatrix} = \begin{pmatrix} \omega r_0 + \Delta_a r_0 & \Delta_M r_0 \\ \Delta_M r_0 & \omega r_0 + \Delta_\parallel r_0 \end{pmatrix} \begin{pmatrix} a \\ E_\parallel \end{pmatrix} = \begin{pmatrix} A(x) & D(x) \\ D(x) & B(x) \end{pmatrix} \begin{pmatrix} a \\ E_\parallel \end{pmatrix}$$

Mixing angle: $\frac{1}{2}\tan 2\theta = \dfrac{D(x)}{B(x) - A(x)}$

$\omega = 100\,\mathrm{keV},\ m_a = 10^{-8}\,\mathrm{keV},$
$r_0 = 10\,\mathrm{km},\ B_0 = 20 \times 10^{14}\,\mathrm{G}$
$g = 10^{-15}\,\mathrm{keV}^{-1},$

$$D(x) = \Delta_M r_0 = \frac{\Delta_{M0} r_0}{x^3} \approx \frac{3.0 \times 10^5}{x^3}$$

$$B(x) = \frac{\Delta_{\parallel 0}\hat{q}(x)}{x^6}\, r_0 \approx \frac{8.6 \times 10^{13}}{x^6}$$

$$A(x) \approx \Delta_a r_0 \approx -2.5 \times 10^{-5}$$

Impossible?

nitude. Although in a detailed calculation of the axion-photon conversion rates the inhomogeneity of the field must be properly included as in our perturbative solution Eq. (33), it is clear that the conversion is now dramatically suppressed due to the magnetically induced vacuum index of refraction. Given this suppression it is difficult to imagine the occurrence of *observable* effects.[36]

Raffelt/Stodolsky (1988)

Solution: n-body

general n-body oscillation problem

$$i\frac{da_i(x)}{dx} = \sum_{j=1}^{n} A_{ij}(x)a_j(x)$$

$$A^*_{ji}(x) = A_{ij}(x) \qquad \frac{d}{dx}\sum_{i=1}^{n}|a_i(x)|^2 = 0$$

$$a_i(x) = \left\{\prod_{j=i}^{n-1}\sin[\chi_j(x)]\right\}\cos[\chi_{i-1}(x)]e^{-i\phi_i(x)}$$

$$\frac{d\chi_{i-1}(x)}{dx} = \sum_{j=1}^{n} A_{ij}(x)S_{ij}(x) + \cot[\chi_{i-1}(x)]\sum_{j=i+1}^{n}\left\{\sum_{\ell=1}^{n} A_{j\ell}(x)S_{j\ell}(x)\right\}\cot[\chi_{j-1}(x)]\left\{\prod_{k=i}^{j-2}\csc^2[\chi_k(x)]\right\}$$

$$\frac{d\phi_i(x)}{dx} = \sum_{j=1}^{n} A_{ij}(x)C_{ij}(x)$$

coefficients

$$S_{ij}(x) = \frac{\left\{\prod_{k=j}^{n-1}\sin[\chi_k(x)]\right\}\cos[\chi_{j-1}(x)]}{\left\{\prod_{k=i}^{n-1}\sin[\chi_k(x)]\right\}\sin[\chi_{i-1}(x)]}\sin[\phi_j(x)-\phi_i(x)],$$

$$C_{ij}(x) = \frac{\left\{\prod_{k=j}^{n-1}\sin[\chi_k(x)]\right\}\cos[\chi_{j-1}(x)]}{\left\{\prod_{k=i}^{n-1}\sin[\chi_k(x)]\right\}\cos[\chi_{i-1}(x)]}\cos[\phi_j(x)-\phi_i(x)].$$

Solution: 2-body

$$i\frac{d}{dx}\begin{pmatrix} a \\ E_{\parallel} \end{pmatrix} = \begin{pmatrix} \omega r_0 + \Delta_a r_0 & \Delta_M r_0 \\ \Delta_M r_0 & \omega r_0 + \Delta_{\parallel} r_0 \end{pmatrix}\begin{pmatrix} a \\ E_{\parallel} \end{pmatrix} = \begin{pmatrix} A(x) & D(x) \\ D(x) & B(x) \end{pmatrix}\begin{pmatrix} a \\ E_{\parallel} \end{pmatrix}$$

$$a(x) = \cos[\chi(x)]e^{-i\phi_a(x)}$$

$$E_{\parallel}(x) = i\sin[\chi(x)]e^{-i\phi_E(x)}$$

$$\frac{d\chi(x)}{dx} + i\cot[\chi(x)]\left[\frac{d\phi_a(x)}{dx} - A(x)\right] = -D(x)e^{i[\phi_a(x)-\phi_E(x)]},$$

$$\frac{d\chi(x)}{dx} - i\tan[\chi(x)]\left[\frac{d\phi_E(x)}{dx} - B(x)\right] = -D(x)e^{-i[\phi_a(x)-\phi_E(x)]}$$

$$\frac{d\chi(x)}{dx} = -D(x)\cos[\Delta\phi(x)],$$

$$\frac{d\Delta\phi(x)}{dx} = A(x) - B(x) + 2D(x)\cot[2\chi(x)]\sin[\Delta\phi(x)].$$

Conversion Probability

$$P_{a\to\gamma}(x) = \sin^2[\chi(x)]$$

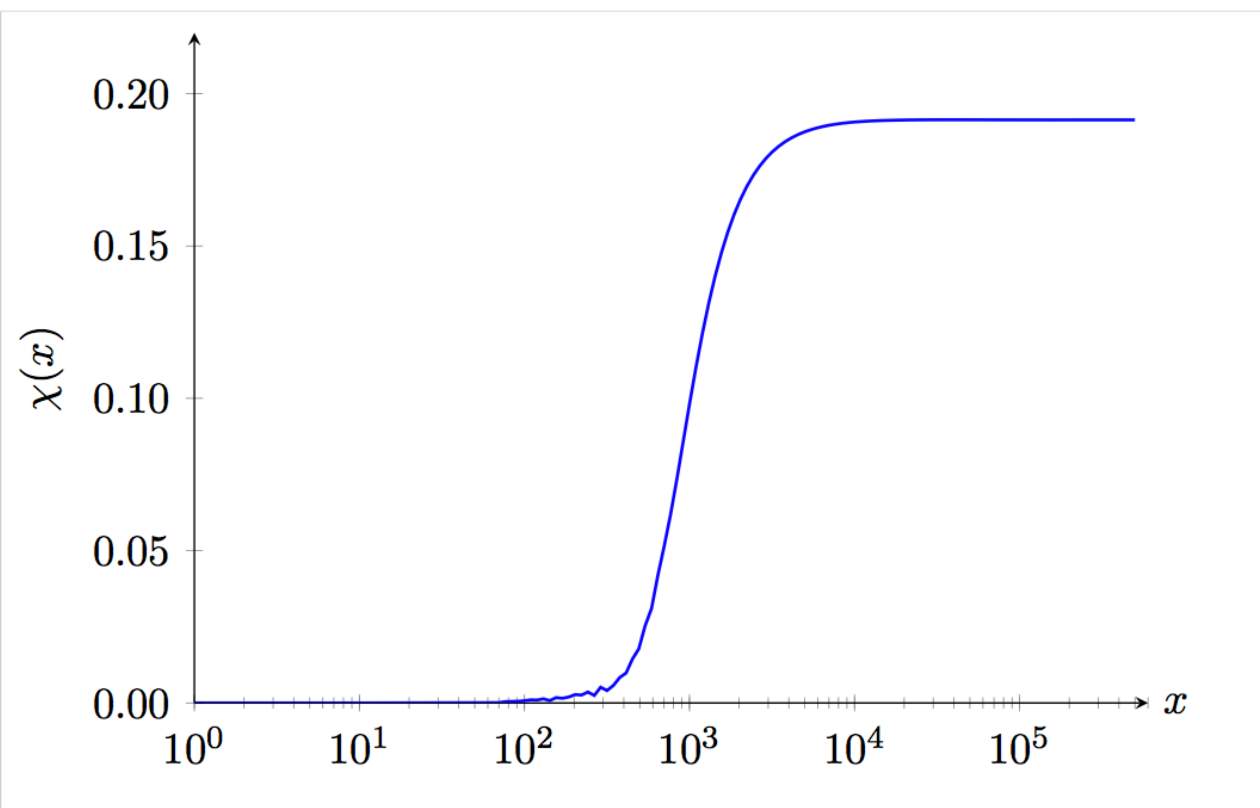

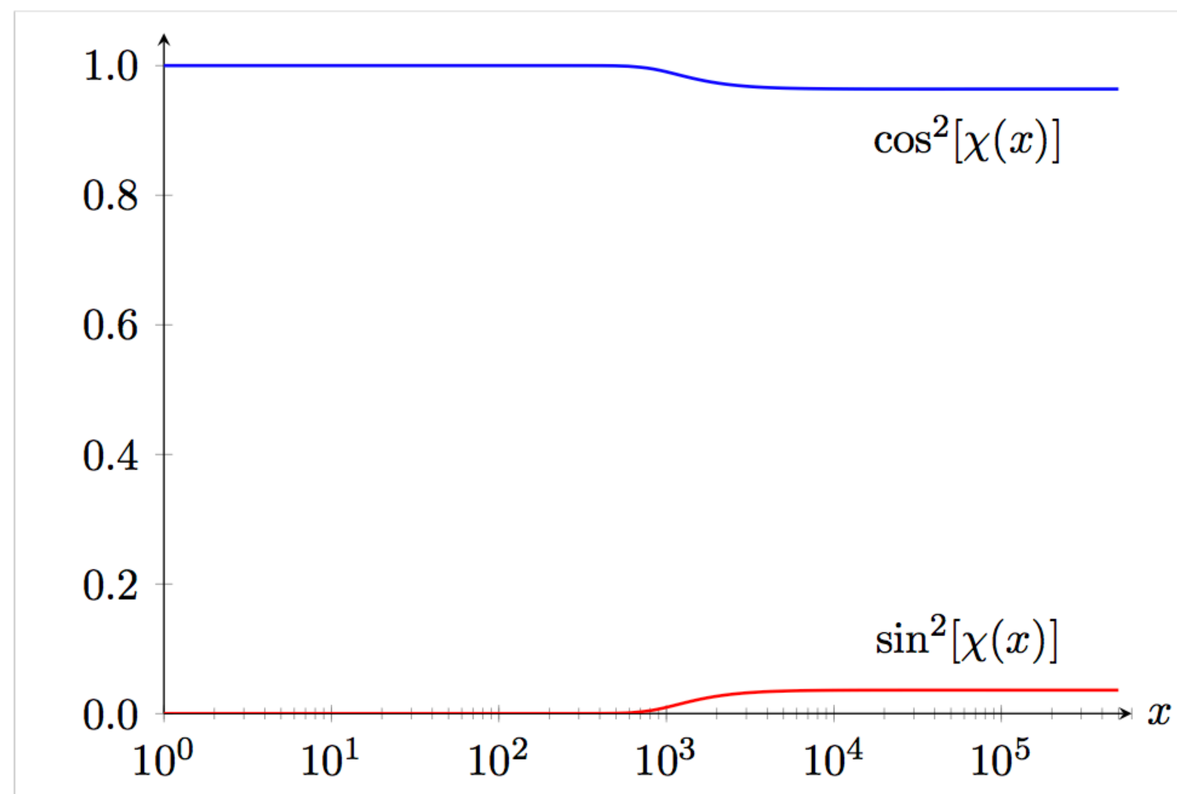

$$\omega = 100\,\mathrm{keV},\ m_a = 10^{-8}\,\mathrm{keV},\ g = 10^{-15}\,\mathrm{keV}^{-1},\ r_0 = 10\,\mathrm{km},\ B_0 = 20\times 10^{14}\,\mathrm{G}$$

Probability Dependences

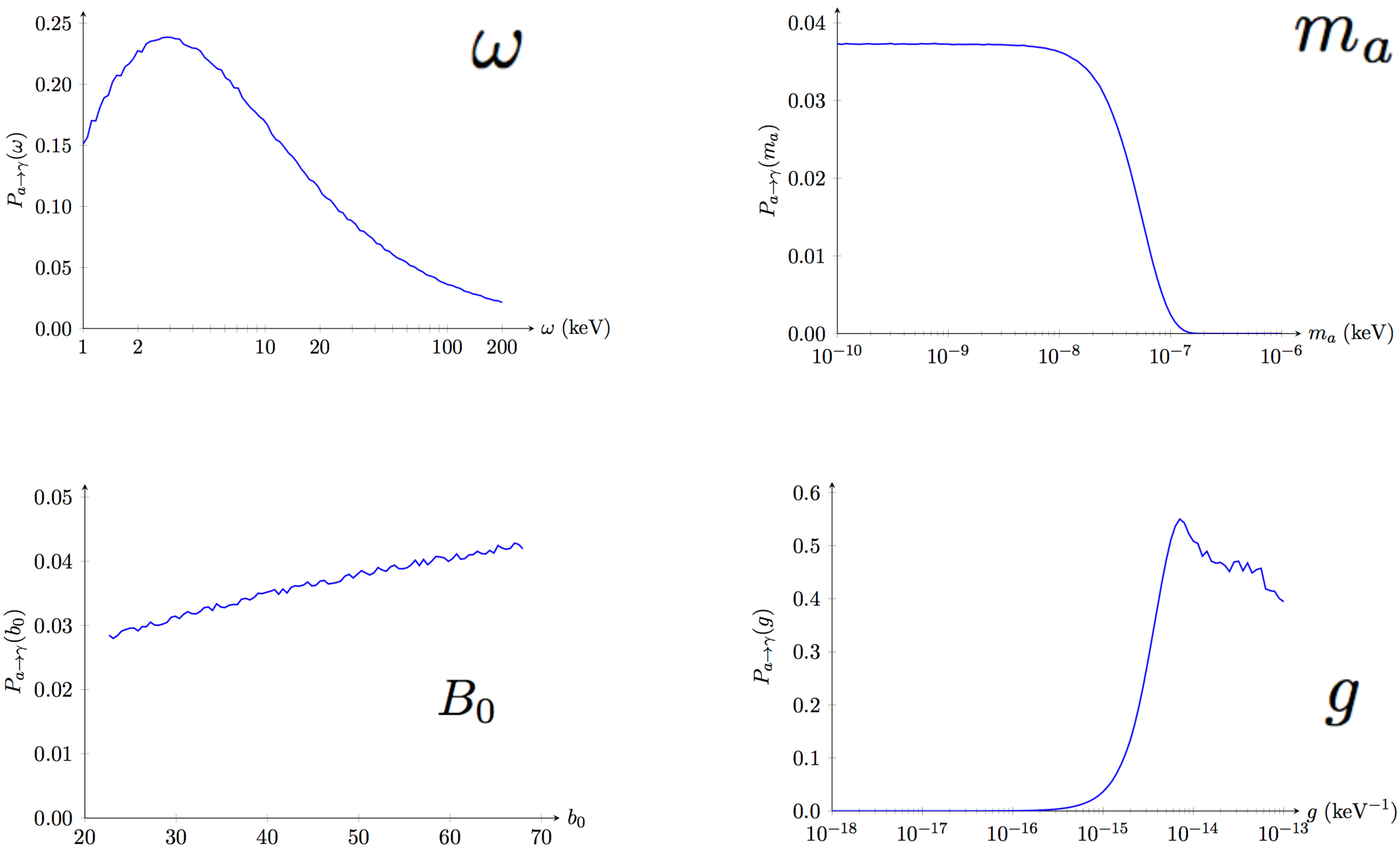

$$\omega = 100\,\text{keV},\ m_a = 10^{-8}\,\text{keV},\ g = 10^{-15}\,\text{keV}^{-1},\ r_0 = 10\,\text{km},\ B_0 = 20 \times 10^{14}\,\text{G}$$

Parameter Scan

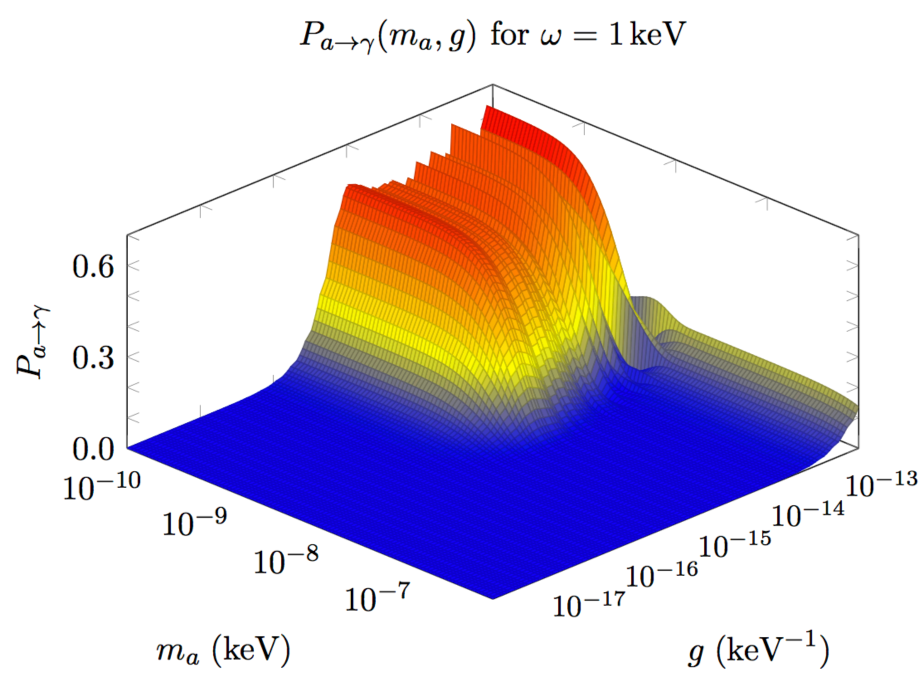

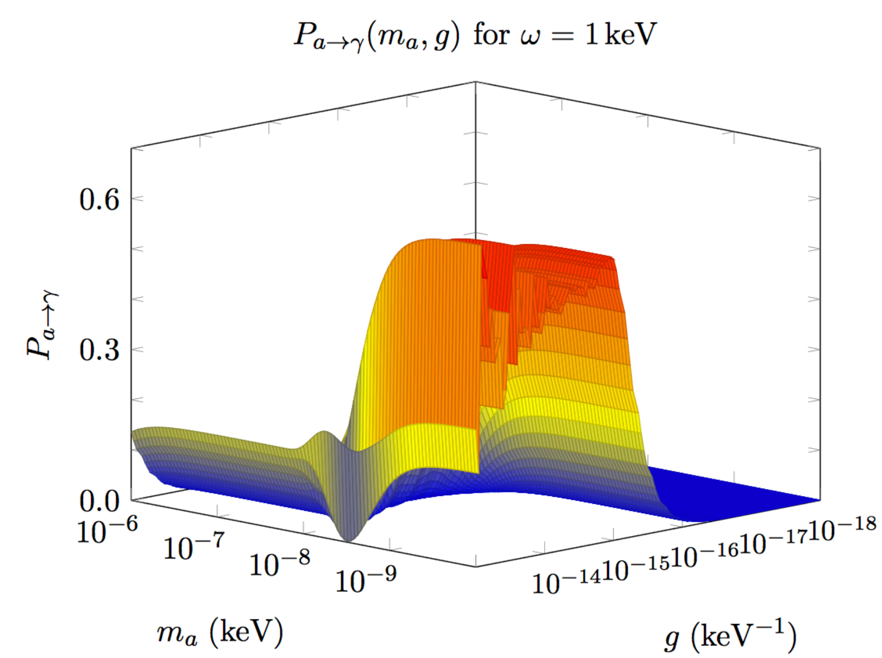

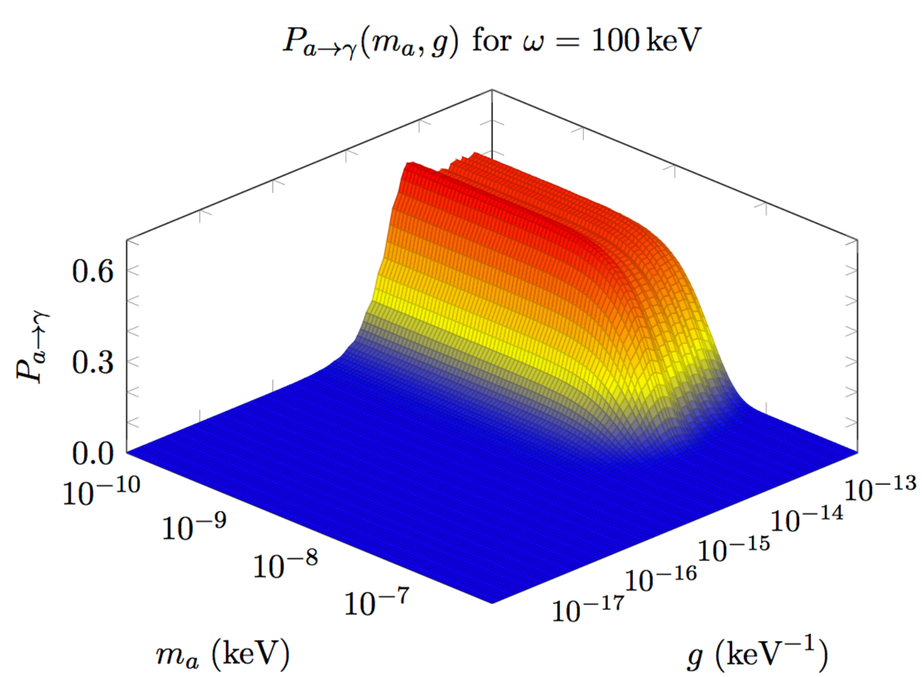

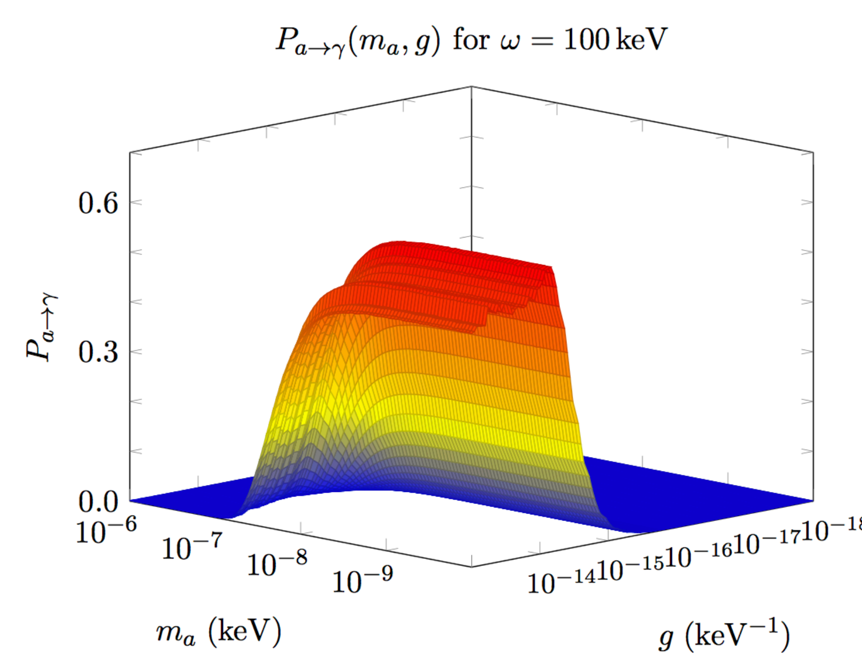

Semi-analytic Treatment

$$P_{a\to\gamma}(x) = \left| \int_1^x dx'\, \Delta_M(x') r_0 \exp\left\{ i \int_1^{x'} dx''\, [\Delta_a - \Delta_{\parallel}(x'')] r_0 \right\} \right|^2$$

$$= (\Delta_{M0} r_0)^2 \left| \int_1^x dx'\, \frac{1}{x'^3} \exp\left[i\Delta_a r_0 \left(x' - \frac{x_{a\to\gamma}^6}{5x'^5} \right) \right] \right|^2 .$$

$$= \left(\frac{\Delta_{M0} r_0^3}{r_{a\to\gamma}^2} \right)^2 \cos(2\chi_0) \times \begin{cases} \frac{\pi}{3|\Delta_a r_{a\to\gamma}|} e^{\frac{6\Delta_a r_{a\to\gamma}}{5}} & |\Delta_a r_{a\to\gamma}| \gtrsim 0.45 \\ \frac{\Gamma\left(\frac{2}{5}\right)^2}{5^{\frac{6}{5}} |\Delta_a r_{a\to\gamma}|^{\frac{4}{5}}} & |\Delta_a r_{a\to\gamma}| \lesssim 0.45 \end{cases}$$

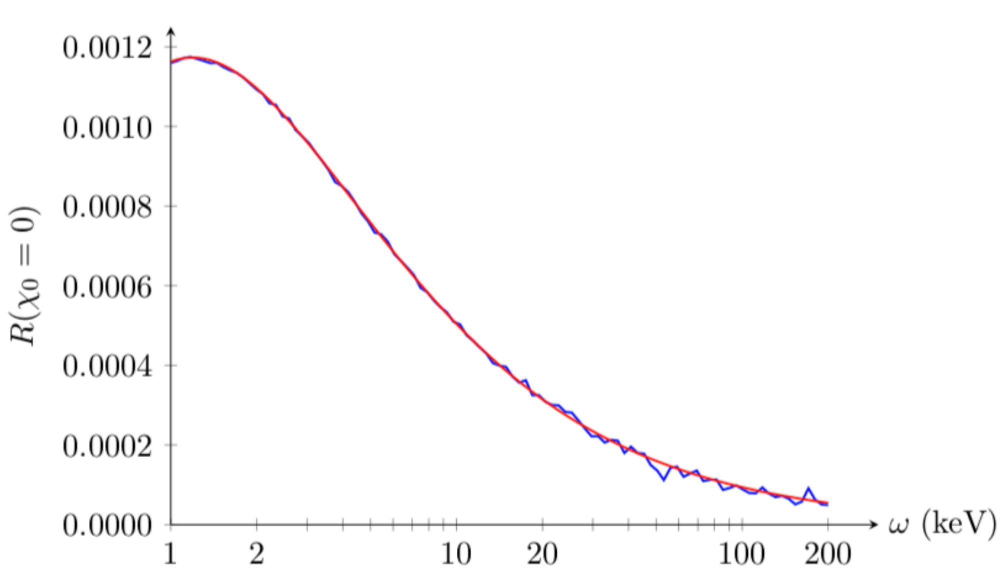

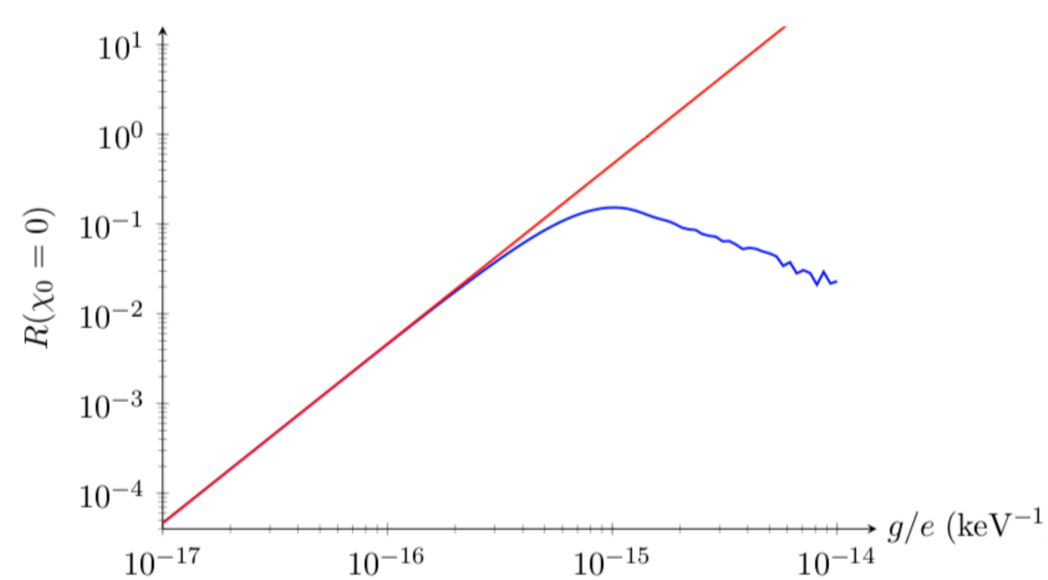

Production
in
Core

Photon Luminosity

$$L_{a\to\gamma} = \frac{N_a}{2\pi}\int_0^{2\pi} d\theta \int_{\omega_i}^{\omega_f} d\omega\, \omega \frac{dN_a}{d\omega} P_{a\to\gamma}(\omega,\theta)$$

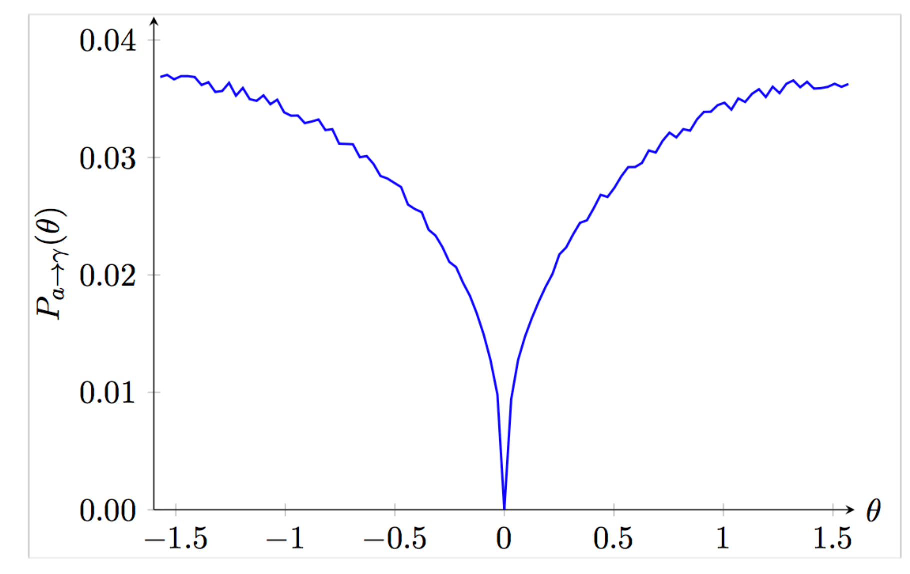

$$\frac{1}{2\pi}\int_0^{2\pi} d\theta\, P_{a\to\gamma}(\omega,\theta) \to R_\theta P_{a\to\gamma}(\omega,\pi/2)$$

$$R_\theta = 0.6$$

total axion number: just subdominant to neutrino cooling

Sedrakian (2017), Balantekin et. al. (2017),…

$$L_a = N_a \int_0^\infty d\omega\, \omega \frac{dN_a}{d\omega} \le L_\nu = 4\pi \int_0^{r_0} dr\, r^2 \dot{q}_\nu$$

ALP Production

$$N_a \leq \frac{4\pi r_0^3 \dot{q}_\nu}{3\int_0^\infty d\omega\, \omega \frac{dN_a}{d\omega}}$$

$$L_{a\to\gamma} = \frac{4\pi r_0^3 \dot{q}_\nu R_\theta}{3\int_0^\infty d\omega\, \omega \frac{dN_a}{d\omega}} \int_{\omega_i}^{\omega_f} d\omega\, \omega \frac{dN_a}{d\omega} P_{a\to\gamma}(\omega, \pi/2)$$

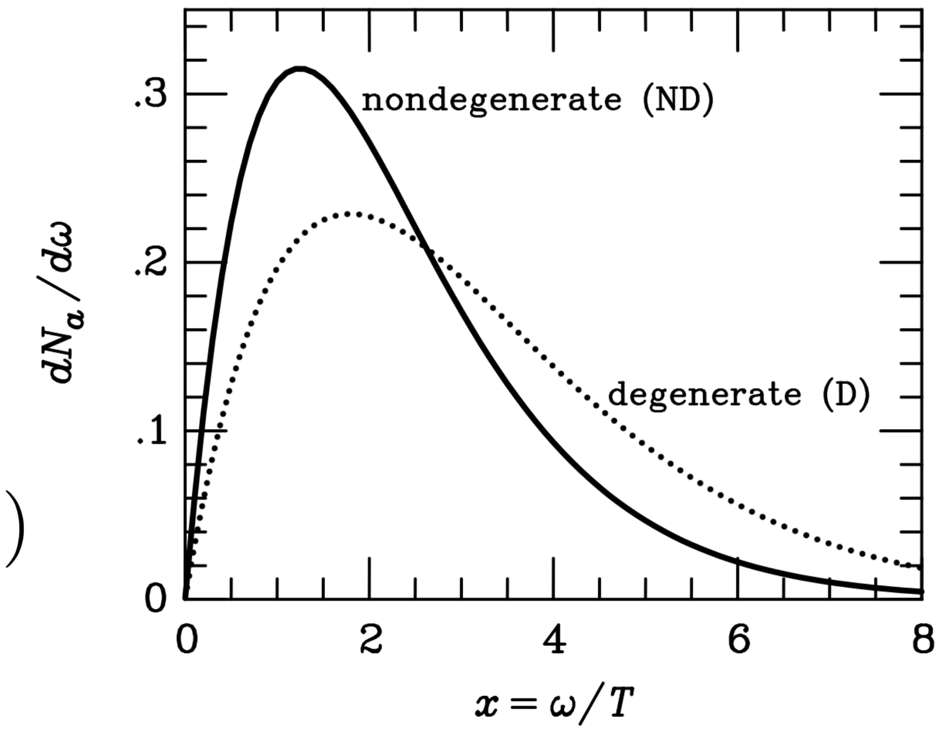

$$\frac{dN_a}{d\omega} = \frac{x^2(x^2+4\pi^2)e^{-x}}{8(\pi^2\zeta_3 + 3\zeta_5)(1-e^{-x})}$$

$\int_0^\infty d\omega\, dN_a/d\omega = 1$

$x = \omega/k_B T$

Iwamoto (1984)
Brinkmann/Turner (1988)
Raffelt (1996)

modified Urca production

$$\dot{q}_\nu = (7\times 10^{20}\,\mathrm{erg}\cdot\mathrm{s}^{-1}\cdot\mathrm{cm}^{-3})\left(\frac{\rho}{\rho_0}\right)^{2/3} R_M \left(\frac{T}{10^9\,\mathrm{K}}\right)^8$$

$\rho_0 = 2.8\times 10^{14}\,\mathrm{g}\cdot\mathrm{cm}^{-3}$ is the nuclear saturation density

Neutrino Cooling

direct Urca

$$\dot{q}_\nu^D \sim 10^{27}\, T_9^6\, \mathcal{R}_D \,\mathrm{erg\ s^{-1}\ cm^{-3}}\ (\rho \gtrsim 10^{15}\,\mathrm{g\ cm^{-3}}),$$

modified Urca

$$\dot{q}_\nu^M \sim 7 \times 10^{20}\, T_9^8 \left(\frac{\rho}{\rho_{\mathrm{nuc}}}\right)^{2/3} \mathcal{R}_M \,\mathrm{erg\ s^{-1}\ cm^{-3}},$$

Cooper pair cooling

$$\dot{q}_\nu^{CP} \sim 10^{21} \left(\frac{\rho}{\rho_{\mathrm{nuc}}}\right)^{1/3} T_9^7\, f\!\left(\frac{T_{\mathrm{core}}}{T_{\mathrm{crit}}}\right) \mathrm{erg\ s^{-1}\ cm^{-3}},$$

Beloborodov (2017)

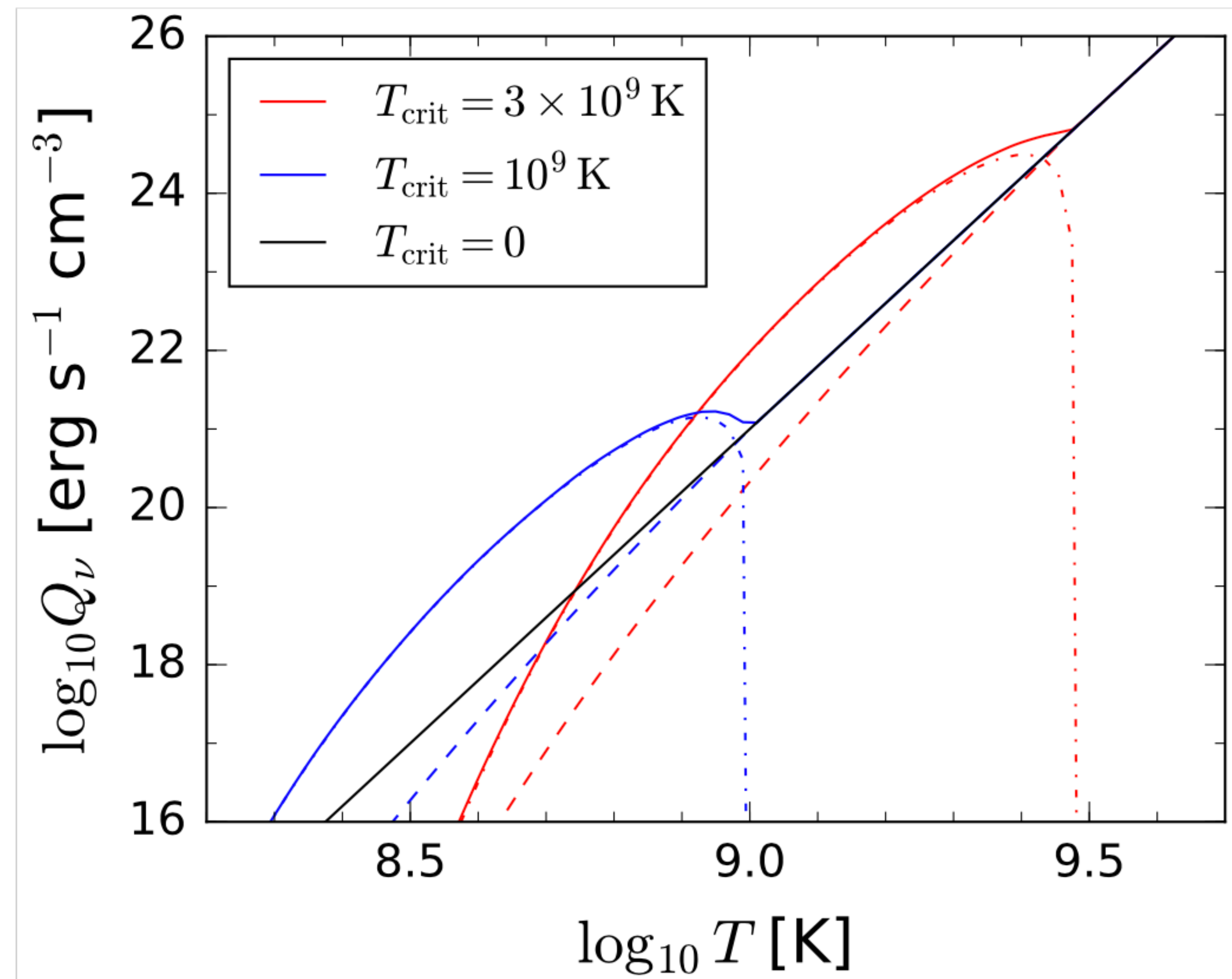

Figure 2. Neutrino cooling rate as a function of temperature in the core at density $\rho_{\mathrm{nuc}} = 2.8 \times 10^{14}$ g cm^{-3}. The black curve shows Murca cooling assuming no superfluidity ($T_{\mathrm{crit}} < 10^8$ K). The colored curves show the cooling of matter with non-superfluid protons and superfluid neutrons, for two cases: $T_{\mathrm{crit}} = 10^9$ K (blue curves) and $T_{\mathrm{crit}} = 3 \times 10^9$ K (red curves). The dashed curve shows the Murca contribution, and the dashed–dotted curve shows the Cooper pair contribution; the net cooling rate is shown by the solid curve. A triplet-state neutron pairing is assumed (model B in Yakovlev et al. 2001).

Core Temperature

$$\dot{q}_\nu = (7 \times 10^{20}\,\mathrm{erg \cdot s^{-1} \cdot cm^{-3}}) \left(\frac{\rho}{\rho_0}\right)^{2/3} R_M \left(\frac{T}{10^9\,\mathrm{K}}\right)^8$$

$$\dot{q}_a = (1.3 \times 10^{25}\,\mathrm{erg \cdot s^{-1} \cdot cm^{-3}}) \left(\frac{g_{aN}}{10^{-10}\,\mathrm{GeV}^{-1}}\right) \left(\frac{\rho}{\rho_0}\right)^{1/3} \left(\frac{T}{10^9\,\mathrm{K}}\right)^6$$

$$\left(\frac{g^*_{aN}}{10^{-10}\,\mathrm{GeV}^{-1}}\right) = 7.3 \times 10^{-3} \left(\frac{\rho}{\rho_0}\right)^{1/6} \sqrt{R_M} \left(\frac{T}{10^9\,\mathrm{K}}\right)$$

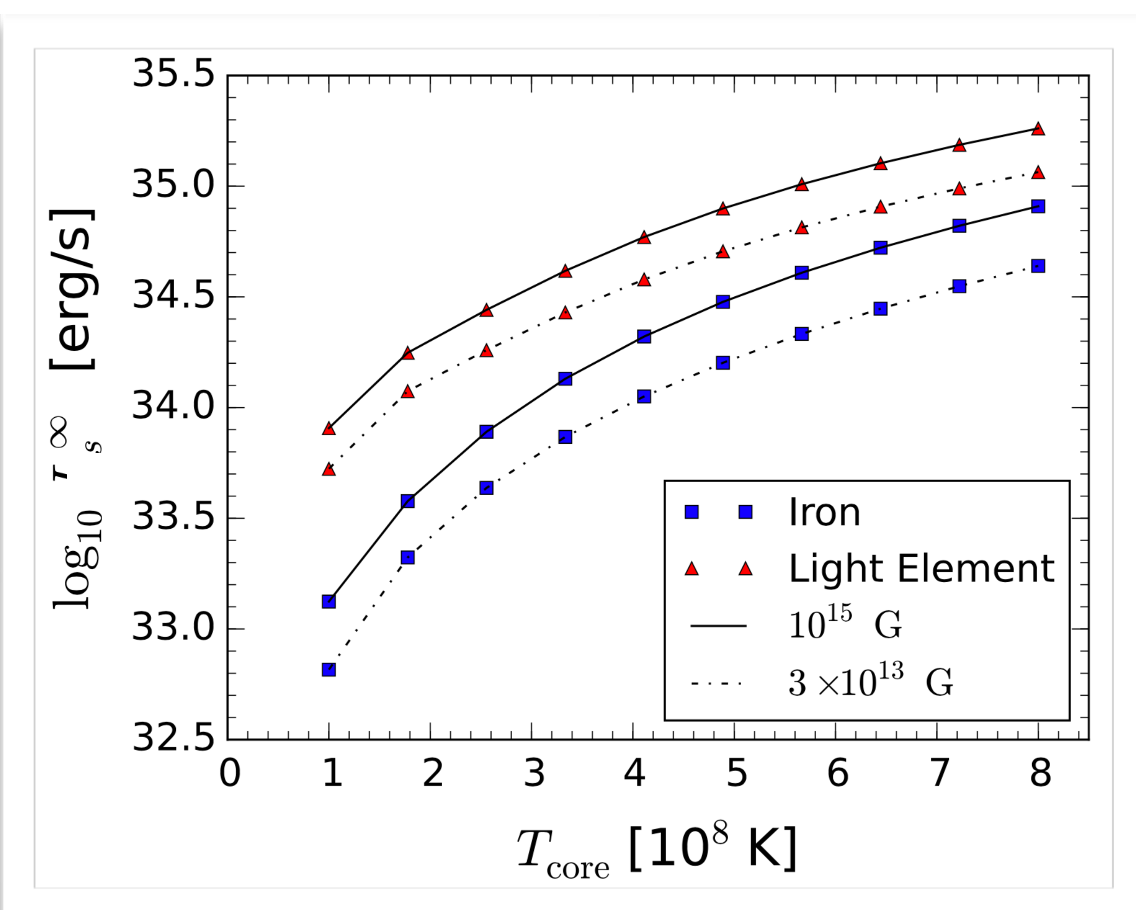

observed at infinity. Each symbol shows a calculated model of steady heat transfer from the core to the stellar surface. The star is assumed to have a dipole magnetic field near the surface, in the heat-blanketing envelope. Two cases are considered: the iron envelope and the maximal light-element envelope, which is called "fully accreted" in Potekhin et al. (2003). The luminosity is shown for two values of the polar magnetic field: $B_p = 3 \times 10^{13}$ G and a more typical one for magnetars $B_p = 10^{15}$ G. As T_core approaches 10^9 K, $\mathcal{L}_s^\infty$ approaches the ceiling imposed by neutrino cooling (Potekhin et al. 2007); heating the core to higher temperatures would not significantly increase the surface luminosity.

Beloborodov/Li (2017)

Total Photon Luminosity

$$L_{a\to\gamma} = \frac{4\pi r_0^3 \dot{q}_\nu R_\theta}{3\int_0^\infty d\omega\,\omega\frac{dN_a}{d\omega}}\int_{\omega_i}^{\omega_f} d\omega\,\omega\frac{dN_a}{d\omega}P_{a\to\gamma}(\omega,\pi/2)$$

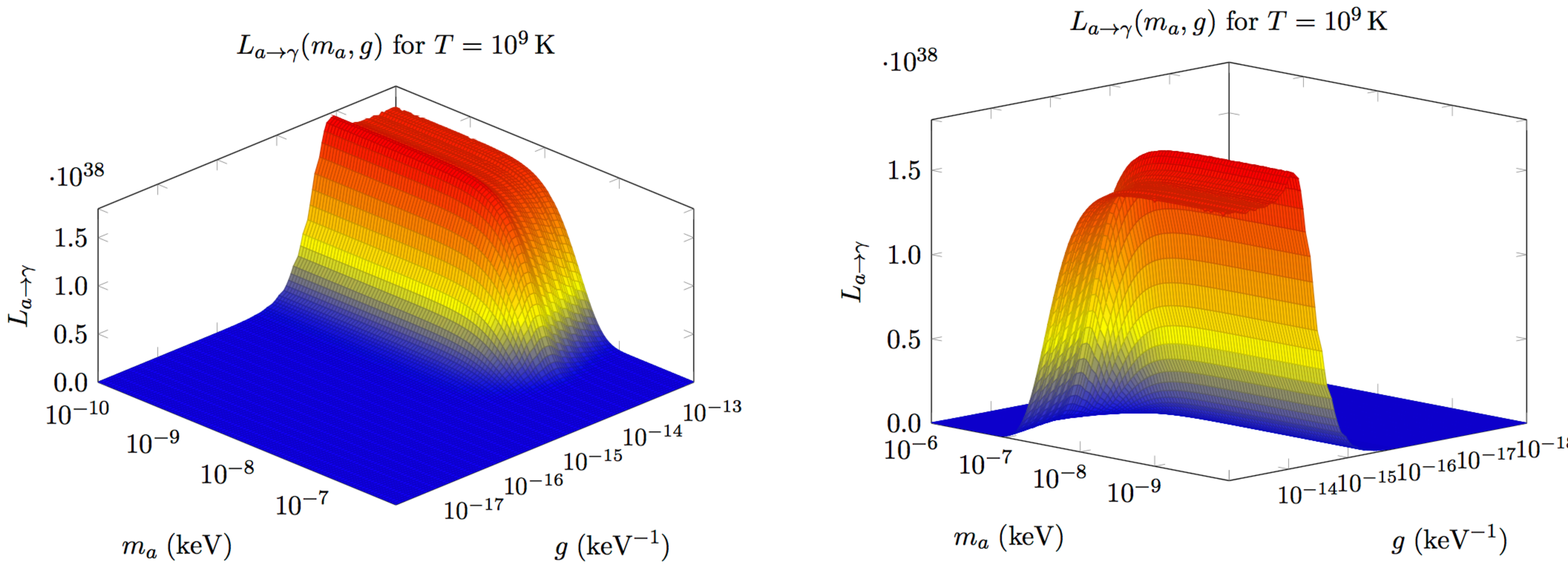

Figure 4. Photon luminosity from ALP-photon oscillations in the broad band from 1 keV to 200 keV in the (m_a, g) plane. The computations are done for SGR 1806-20 assuming $r_0 = 10$ km and $B_0 = 20\times10^{14}$ G. The magnetar core temperature is assumed to be $T = 10^9$ K. The two panels show the same conversion probability from different points of view.

Comparison with Observations

Non-thermal Emission

Besides spectacular outbursts, magnetars produce persistent or decaying X-ray emission with luminosity $L \sim 10^{34} - 10^{36}$ erg s^{-1}. Two peaks are observed in their X-ray spectra, with comparable luminosities. The first peak is near 1 keV; it is associated with thermal emission from the neutron star surface. The second peak is above 100 keV. Its low-energy slope (between 10 and 100 keV) was observed in 7 magnetars[1] (Kuiper et al. 2008; Enoto et al. 2010), with a typical photon index $\Gamma \sim 1 - 1.5$.

Beloborodov (2012)

SGR 1806-20

Name[b]	P (s)	B[c] (10^{14} G)	Age[d] (kyr)	$\dot{E}$[e] 10^{33} erg s^{-1}	D[f] (kpc)	L_X[g] 10^{33} erg s^{-1}	Band[h]
SGR 1806−20	7.55	20	0.24	45	8.7	163	OIR/H

1200

Kaspi (2016)

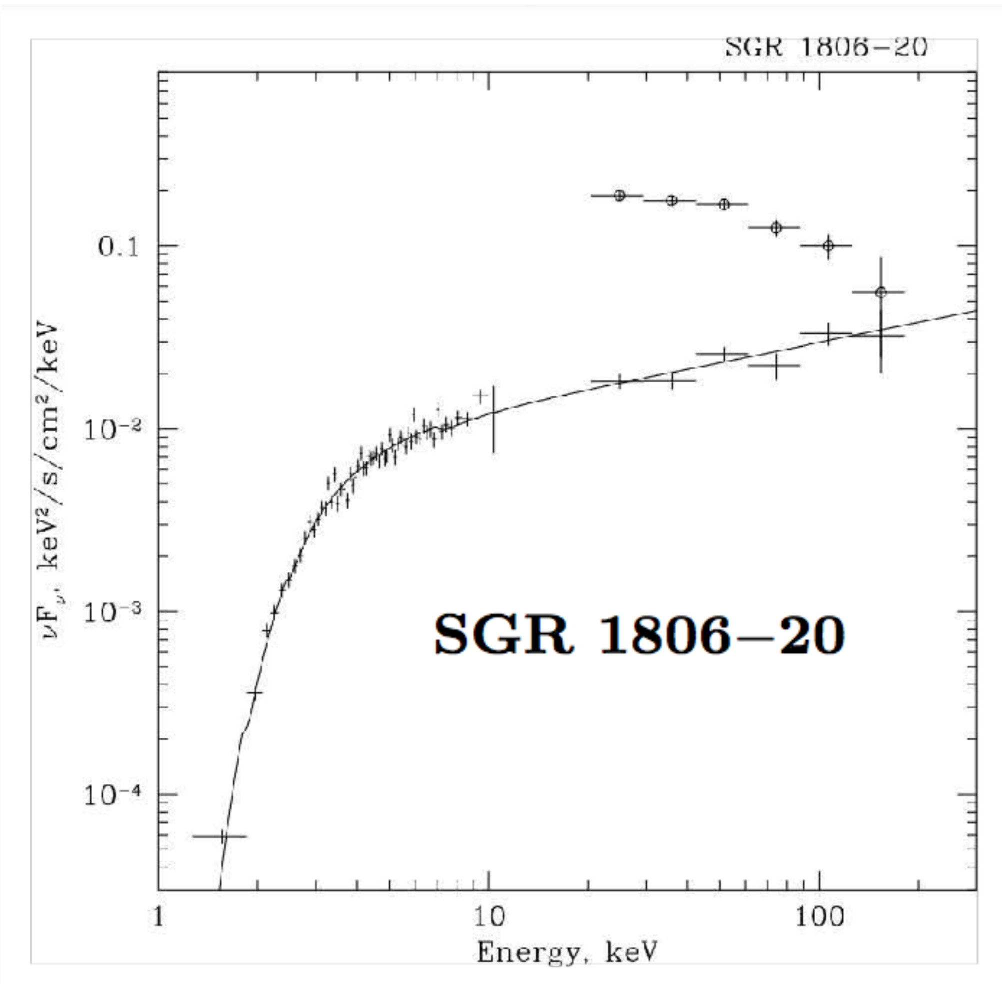

Sunyaev et. al. (2004)

In this letter we present the broad band spectrum (1-200 keV) of the persistent emission of SGR 1806-20 ob-

tory in autumn 2003. The source flux was $\sim 1.3 \times 10^{-10}$ erg s^{-1} cm^{-2}, which corresponds to a source luminosity $\sim 3.6\times10^{36}$ erg s^{-1} in this energy band (assuming a source

McGill Online Magnetar Catalog

Table 4: Hard X-ray observations

- This table is available in ASCII and CSV format.
- Back to main catalog.

Name	Cutoff Energy	PL Index (Pulsed)	Pulsed F_x{a}	PL Index (Total)	Total F_x{a}	Telescope	Ref.{b}
	(keV)		(10^{-11} erg/s/cm^2)		(10^{-11} erg/s/cm^2)		
4U 0142+61	279^{+65}_{-41} [dkh+08]	0.40(15) …	2.68(1.34) …	0.93(6) $0.89^{+0.11}_{-0.10}$	9.09(35) 10.3 [$3.28^{+0.32}_{-0.29}$ (15–60 keV)]	Integral, RXTE Suzaku	[dkh+08] [emn+11]
SGR 0501+4516	>100 [rit+09]	… … …	… … …	0.8(2) … $0.79^{+0.20}_{-0.18}$	… <3.5 [<0.97 (18–60 keV)] $8.4^{+2.0}_{-1.5}$ [$4.8^{+0.8}_{-0.6}$ (20–100 keV)]	Integral Integral Suzaku	[rit+09] [rit+09] [ern+10]
1E 1547.0−5408	>200 [enm+10a]	… $-0.37^{+0.28}_{-0.20}$ $-0.59^{+0.25}_{-0.19}$ $-1.55^{+0.42}_{-0.26}$ … … … … … …	… $6.9^{+1.2}_{-1.0}$ $7.5^{+0.9}_{-1.0}$ 4.1(9) … … … … … …	$1.54^{+0.06}_{-0.05}$ … … … … 1.41(6) 1.45(4) 1.27(11) 1.22(10) 0.87(7)	$17.4^{+1.4}_{-1.8}$ [$12.5^{+0.8}_{-1.1}$ (20–100 keV)] … … … <1.5 25.2(3.7) 18.5(1.8) 21.5(1.4) 8.4(2.7) 8.0(2.2)	Suzaku RXTE RXTE RXTE Integral Integral Integral Integral Integral Integral	[enm+10a] [khdu12] [khdu12] [khdu12] [khdu12] [khdu12] [khdu12] [khdu12] [khdu12] [khdu12]
1RXS J170849.0−400910	>300 [dkh08]	… 0.86(16)	… 2.60(35)	1.46(21) 1.13(6)	5.2(1.0) [3.6(5) (20–100 keV)] 6.61(23)	Integral Integral, RXTE	[gri+07] [dkh08]
SGR J1745−2900	>50 [mgz+13]	…	…	$1.47^{+0.46}_{-0.37}$	$0.67^{+0.20}_{-0.26}$ [0.622(57) (2–79 keV)]	NuSTAR	[mgz+13]
SGR 1806−20	>160 [mhs+05]	… … … … …	… … … … …	1.9(2) 1.5(3) 1.7(1) 1.2(1) 1.6(2)	6.0(9) [4.7(5) (20–100 keV)] 11(2) [8(9) (20–100 keV)] 4.70 [$5.56^{+0.31}_{-0.23}$ (1–60 keV)] 9.89 [$5.71^{+0.65}_{-0.60}$ (1–60 keV)] 3.83 [$3.86^{+0.40}_{-0.77}$ (1–60 keV)]	Integral Integral Suzaku Suzaku Suzaku	[mgmh05] [mgmh05] [enm+10b] [enm+10b] [enm+10b]
1E 1841−045	>140 [khdc06]	0.72(15) $1.35^{+0.30}_{-0.25}$ 0.99(36)	4.00 [2.44 (10–100 keV)] 2.67 [$2.18^{+0.62}_{-0.51}$ (1–50 keV)] 3.03 [1.76(27) (3–79 keV)]	1.32(11) $1.62^{+0.21}_{-0.22}$ 1.33(3)	6.88 [5.54 (10–100 keV)] 4.59 [$4.37^{+0.39}_{-0.29}$ (1–50 keV)] 7.99 [6.84(6) (3–79 keV)]	Integral, RXTE Suzaku NuSTAR	[khdc06] [mks+10] [ahk+13]
SGR 1900+14	>100 [gmte06]	… … …	… … …	3.1(5) 1.2(5) 1.4(3)	1.6(4) [1.5(3) (20–100 keV)] 3.24 [$1.87^{+0.40}_{-0.77}$ (1–60 keV)] 1.42 [$1.07^{+0.24}_{-0.21}$ (1–60 keV)]	Integral Suzaku Suzaku	[gmte06] [enm+10b] [enm+10b]

Results

$$L_\gamma^{\rm obs} = 1.2 \times 10^{36}\,{\rm erg}\cdot{\rm s}^{-1}$$

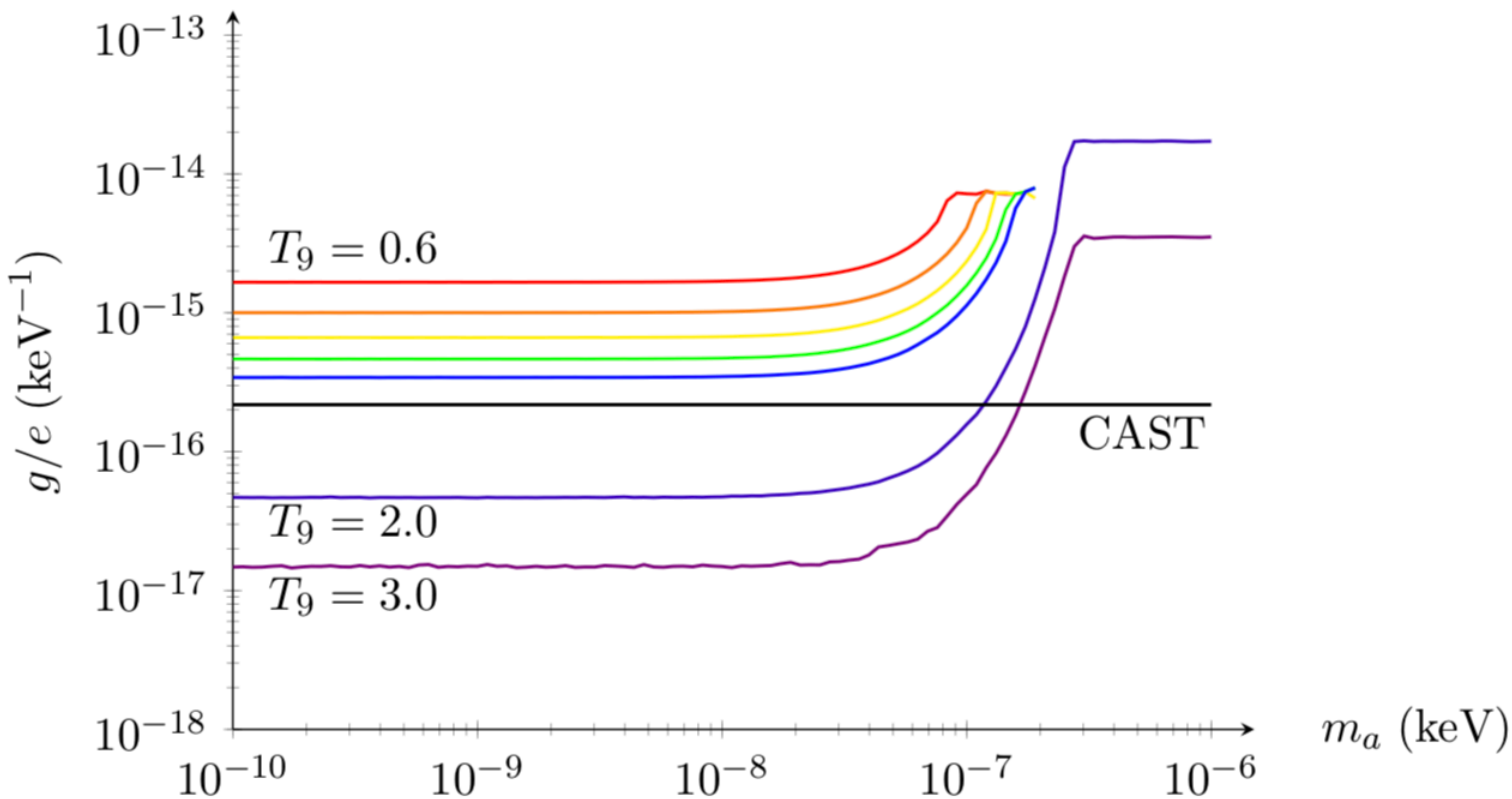

m_a (keV)

Polarization

X-mode Domination

Lai/Ho (2003), Heyl/Lai (2007)

Electron cyclotron frequency: $\omega_{ce} = m_e(B/B_c) \sim 50 \text{ MeV}$

$$\omega \ll \omega_{ce}$$

Description in terms of X-mode and O-mode

$$\frac{I_{\|}(\chi_0, x=1)}{I_{\perp}(x=1)} \sim (\omega/\omega_{ce})^2 \sim 10^{-6}$$

Most of the thermal radiation is X-mode

QED Effect

$$i\frac{d}{dr}\begin{pmatrix} E_{\parallel} \\ E_{\perp} \end{pmatrix} = \frac{\omega}{2}\begin{pmatrix} 2+\sigma_{11} & \sigma_{12} \\ \sigma_{21} & 2+\sigma_{22} \end{pmatrix}\begin{pmatrix} E_{\parallel} \\ E_{\perp} \end{pmatrix}$$

$$\sigma_{12} = -\sigma_{21} \sim 0 \qquad \sigma_{11} \sim (q_{\parallel} - \frac{\omega_{pl}^2}{\omega^2})\sin^2\theta \qquad \sigma_{22} \sim -q_{\perp}\sin^2\theta$$

QED contribution

$$q_{\parallel} = \frac{7\alpha}{45\pi} b^2 \hat{q}_{\parallel}$$

$$q_{\perp} = \frac{4\alpha}{45\pi} b^2 \hat{q}_{\perp}$$

Plasma contribution

$$\omega_{pl}^2 = 4\pi e^2 n_e / m_e$$

electron density

electron fraction

$$n_e = Y_e \rho / m_p$$

mass density

proton mass

Vacuum Resonance

$$i\frac{d}{dr}\begin{pmatrix} E_{\|} \\ E_{\perp} \end{pmatrix} = \frac{\omega}{2}\begin{pmatrix} 2+\sigma_{11} & \sigma_{12} \\ \sigma_{21} & 2+\sigma_{22} \end{pmatrix}\begin{pmatrix} E_{\|} \\ E_{\perp} \end{pmatrix}$$

$$\sigma_{12} = -\sigma_{21} \sim 0 \qquad \sigma_{11} \sim \left(q_{\|} - \frac{\omega_{pl}^2}{\omega^2}\right)\sin^2\theta \qquad \sigma_{22} \sim -q_{\perp}\sin^2\theta$$

$$\boxed{\sigma_{11} = \sigma_{22}}$$

$$\frac{\omega_{pe}^2}{\omega^2} = q_{\|} + q_{\perp} \quad \Rightarrow \quad \rho \sim 0.964 Y_e^{-1}\left(\frac{\omega}{1\,\mathrm{keV}}\frac{B}{10^{14}\,\mathrm{G}}\right)^2$$

X-modes in Hard X-rays

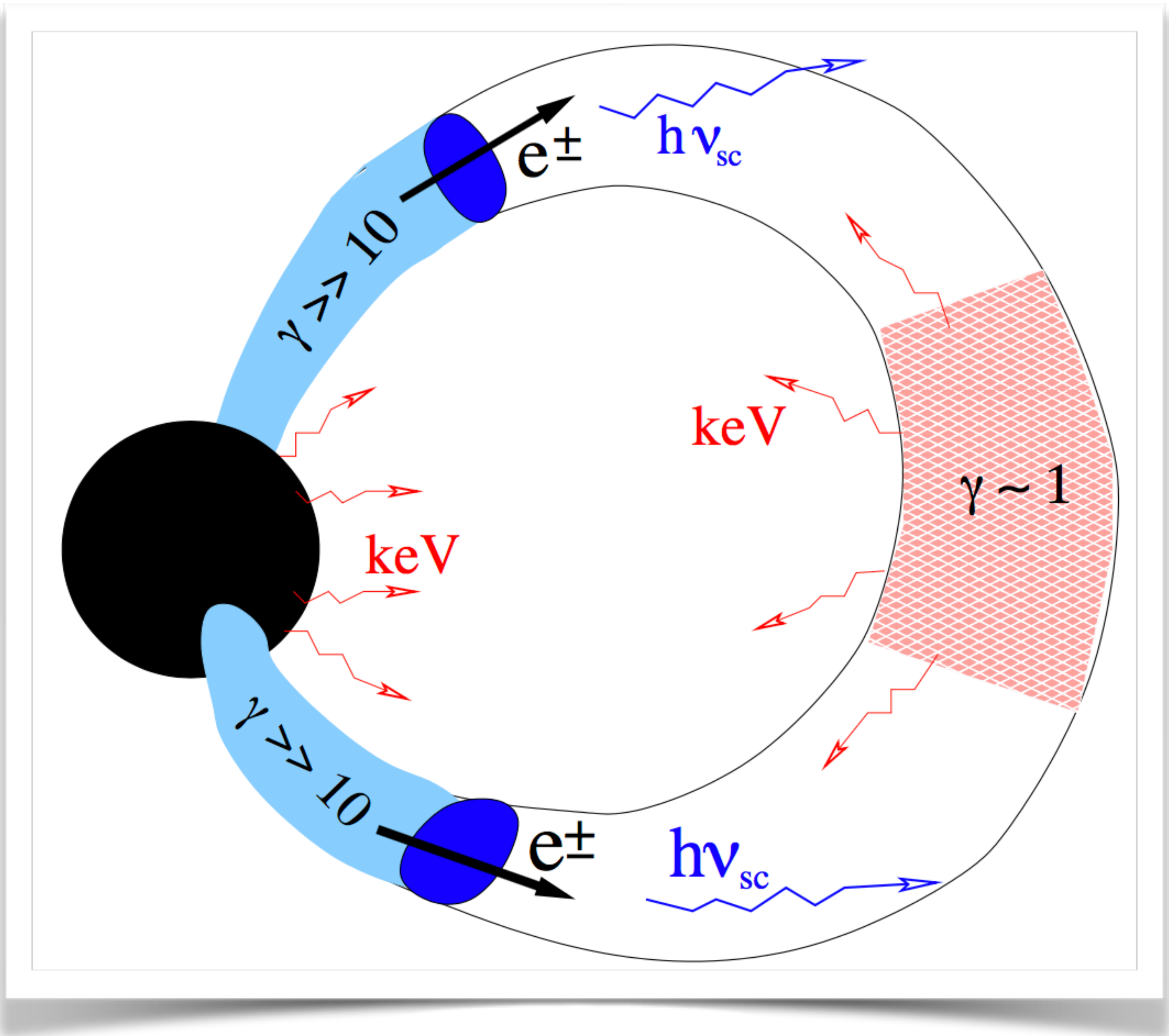

Beloborodov (2012)
Baring (2017)

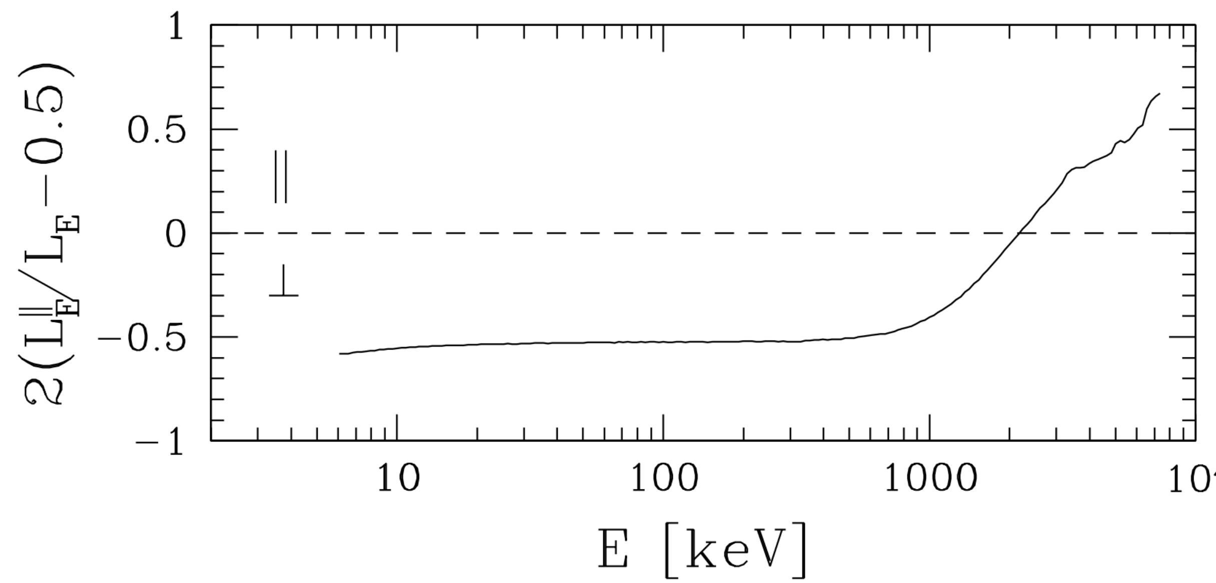

Net 75% polarization in X-mode

X-modes in Hard X-rays

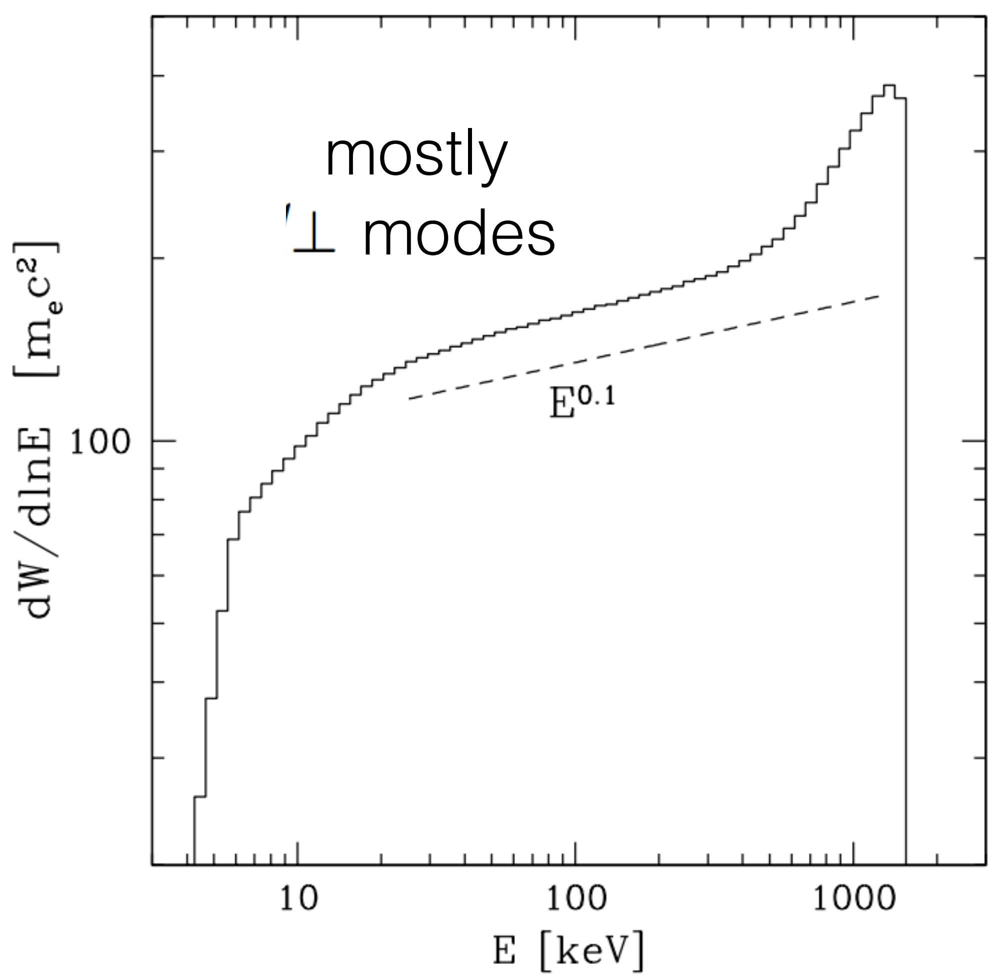

Figure 5. Average spectrum of escaping radiation from cascades generated by primary particles with Lorentz factor $\gamma_p = 10^3$. The total emitted energy W equals the injected energy $\gamma_p m_e c^2$. Dashed line shows the analytical estimate (Equation 20). Photon splitting creates an additional bump that is visible at $E \sim 1$ MeV. The bump consists of photons with $\parallel$ polarization. Emission at lower energies $E \ll 1$ MeV is dominated by photons with $\perp$ polarization.

Beloborodov (2012)

- Relativistic plasma ejected from magnetar; Large Lorentz factors.

$$\Phi \sim 10^9 \text{ V}$$

$$\gamma \sim e\Phi/m_e c^2 \sim 10^3$$

- Resonantly scatters with thermal keV photons
Photon energy in e rest frame = Landau energy

$$\tilde{E} = \hbar\omega_B = b\, m_e c^2$$

- Photons get tremendous energy boost. Parallel modes convert into e+e- pairs via pair production; perp modes undergo photon splitting for energies above 1 MeV. The two produced photons have parallel polarization and split into e+e-. Both modes thus reprocessed into e+e-; trapped.

- When B < 0.01B_crit, photons escape. Pink region. Mostly perpendicular modes.

- Photon of energy E is emitted where $b \approx 0.1(E/m_e c^2)^{1/2}$ For our case, x ~ 8

Polarization Radius

Heyl (2016)

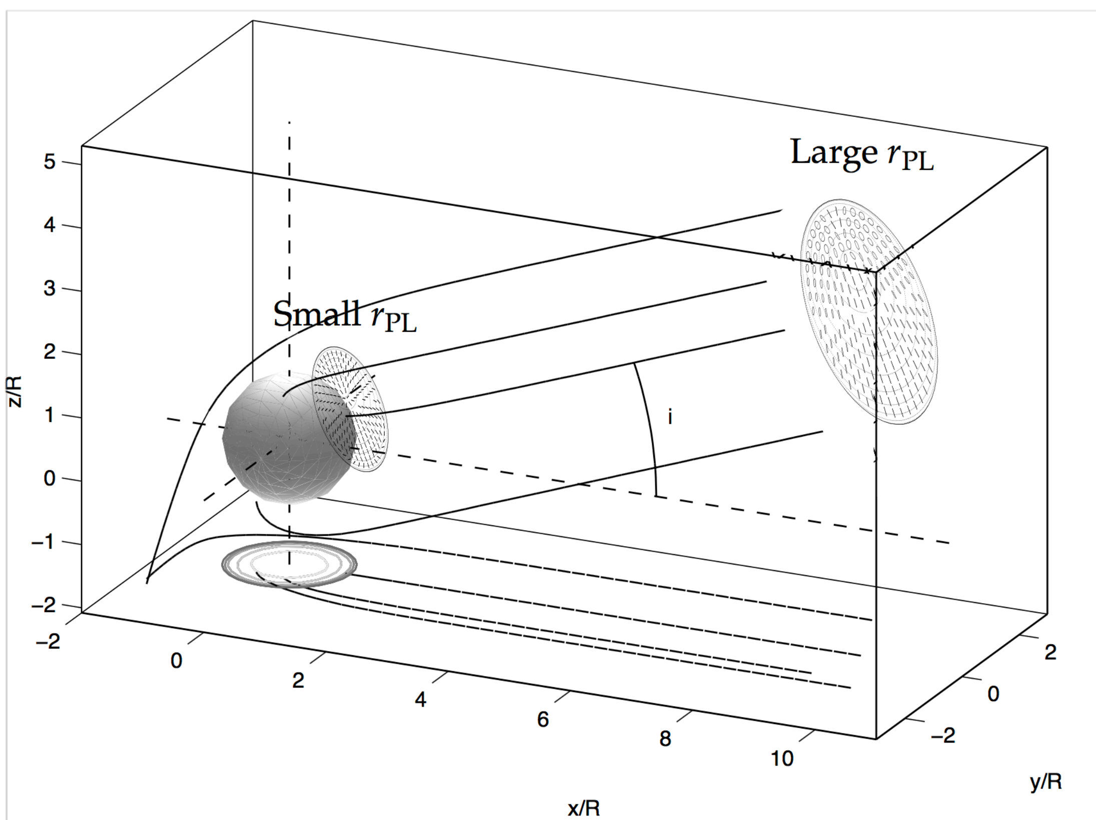

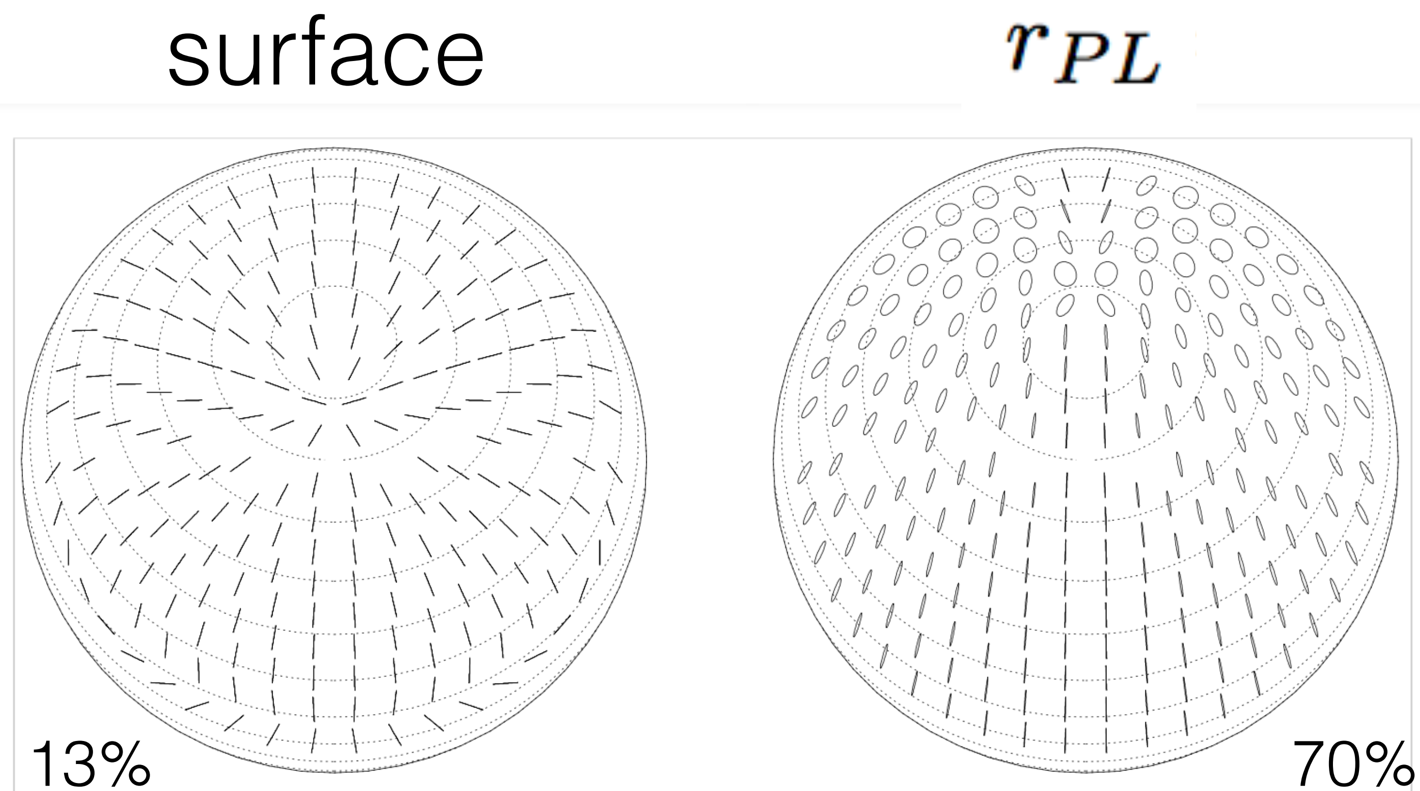

$$r_{PL} = \left(\frac{\alpha}{45}\frac{\nu}{c}\right)^{1/5}\left(\frac{B_0}{B_c}r_0^3\sin\beta\right)^{2/5} \sim 923.4\left(\frac{\omega}{1\,\mathrm{keV}}\right)^{1/5}\left(\frac{B_0}{10^{14}\,\mathrm{G}}\right)^{2/5}\left(\frac{r_0}{10\,\mathrm{km}}\right)^{6/5}\mathrm{km},$$

$$\boxed{r_{PL} \sim 300\, r_0}$$

O-Modes from ALPs

$$i\frac{d}{dx}\begin{pmatrix} a \\ E_{\|} \\ E_{\perp} \end{pmatrix} = \begin{pmatrix} \omega r_0 + \Delta_a r_0 & \Delta_M r_0 & 0 \\ \Delta_M r_0 & \omega r_0 + \Delta_{\|} r_0 & 0 \\ 0 & 0 & \omega r_0 + \Delta_{\perp} r_0 \end{pmatrix} \begin{pmatrix} a \\ E_{\|} \\ E_{\perp} \end{pmatrix}$$

$$\Delta_a = -\frac{m_a^2}{2\omega}, \qquad \Delta_{\|} = \frac{1}{2} q_{\|} \omega \sin^2\theta, \qquad \Delta_{\perp} = \frac{1}{2} q_{\perp} \omega \sin^2\theta, \qquad \Delta_M = \frac{1}{2} g B \sin\theta.$$

$$a(x) = A\cos[\chi(x)]e^{-i\phi_a(x)}$$

axion

$$E_{\|}(x) = iA\sin[\chi(x)]e^{-i\phi_{\|}(x)}$$

O-mode

$$E_{\perp}(x) = A_{\perp} e^{-i\phi_{\perp}(x)}$$

X-mode

ALP-O-mode Evolution

ALP + O-mode evolution

$$\frac{d\chi(x)}{dx} = -\Delta_M r_0 \cos[\Delta\phi(x)],$$

$$\frac{d\Delta\phi(x)}{dx} = (\Delta_a - \Delta_{||})r_0 + 2\Delta_M r_0 \cot[2\chi(x)] \sin[\Delta\phi(x)]$$

Sum of phases:

$$\frac{d\Sigma\phi(x)}{dx} = (2\omega + \Delta_a + \Delta_{||})r_0 - 2\Delta_M r_0 \csc[2\chi(x)] \sin[\Delta\phi(x)],$$

X-mode evolution

$$\frac{d\phi_\perp(x)}{dx} = (\omega + \Delta_\perp)r_0$$

Initial Conditions

Intensities:

$$I_a(x) = A^2 \cos^2[\chi(x)] \qquad I_{||}(x) = A^2 \sin^2[\chi(x)] \qquad I_\perp(x) = A_\perp^2$$

axion O-mode X-mode

Free initial conditions:

$$\chi(1) = \chi_0 \qquad I_{||}(1) \qquad I_\perp(1)$$

Uncorrelated ALP+O-mode states

integrate over $\Delta\phi(1) = \Delta\phi_0$

Averaged Stokes Parameters

Phase-averaged intensities at position x:

$$\bar{I}_a(\chi_0, x) = \int_0^{2\pi} \frac{d\Delta\phi_0}{2\pi} I_a(\chi_0, \Delta\phi_0, x)$$

axion

$$\bar{I}_{||}(\chi_0, x) = \int_0^{2\pi} \frac{d\Delta\phi_0}{2\pi} I_{||}(\chi_0, \Delta\phi_0, x)$$

O-mode

Stokes parameters

$$I(\chi_0, x) = \bar{I}_\perp(x) + \bar{I}_{||}(\chi_0, x)$$

$$Q(\chi_0, x) = \bar{I}_\perp(x) - \bar{I}_{||}(\chi_0, x)$$

Closed analytic form?

Q Behavior

$$Q(\chi_0, x) = A_\perp^2 - \frac{A^2}{2}\left\{1 + [2P_{a\to\gamma}(x) - 1]\cos(2\chi_0)\right\}$$

X-mode

O-mode

Conversion probability

Initial condition

$\chi_0 \;=\; 0$ (if there are no O-modes at the surface)

$\bar{I}_{||}/\bar{I}_\perp \sim 0$ assume only X-modes produced astrophysically

$\bar{I}_a/\bar{I}_\perp \sim 0 - \mathcal{O}(10^4)$ no ALPs to limit from luminosity

Q Behavior

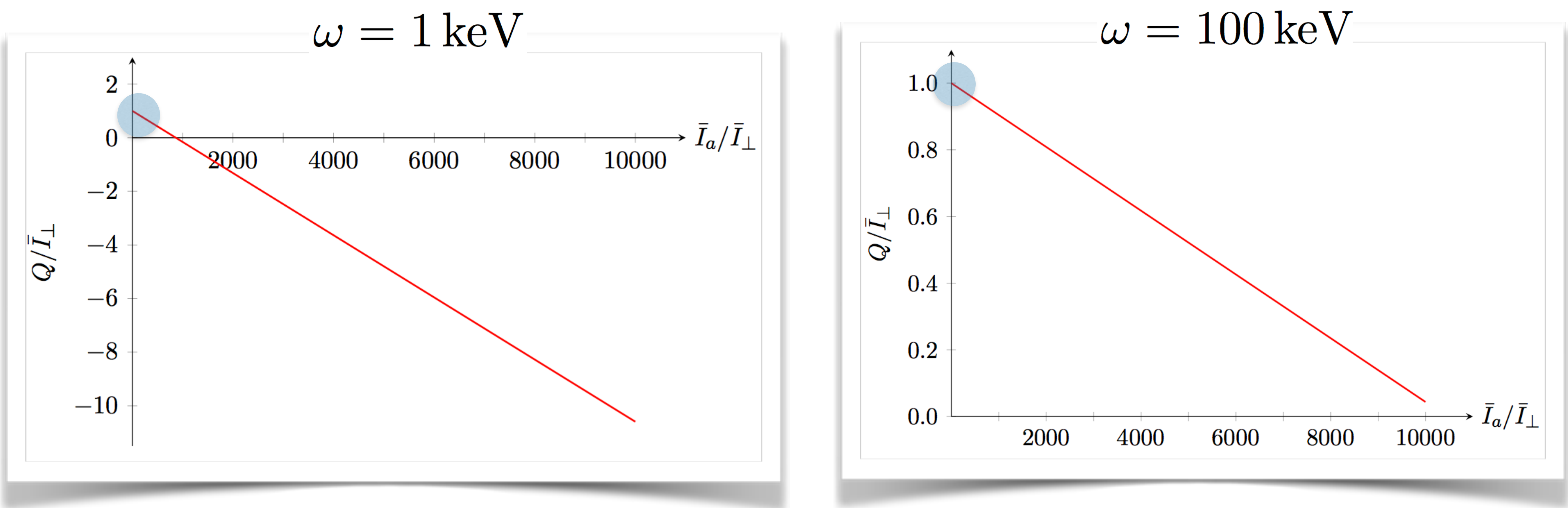

Fig. 4: (Normalized) Stokes parameter $Q/\bar{I}_\perp$ at infinity for the benchmark point $m_a = 10^{-8}\,\mathrm{keV}$, $g = 5\times10^{-17}\,\mathrm{keV}^{-1}$, $r_0 = 10\,\mathrm{km}$, $B_0 = 20\times10^{14}\,\mathrm{G}$ and $\theta = \pi/2$ in function of $\bar{I}_a/\bar{I}_\perp$ at the surface assuming $\bar{I}_\parallel/\bar{I}_\perp \sim 0$ at the surface. The left panel corresponds to ALP energy $\omega = 1\,\mathrm{keV}$ ($P_{a\to\gamma} \approx 1.2\times10^{-3}$) while the right panel corresponds to $\omega = 100\,\mathrm{keV}$ ($P_{a\to\gamma} \approx 9.6\times10^{-5}$).

Q Behavior

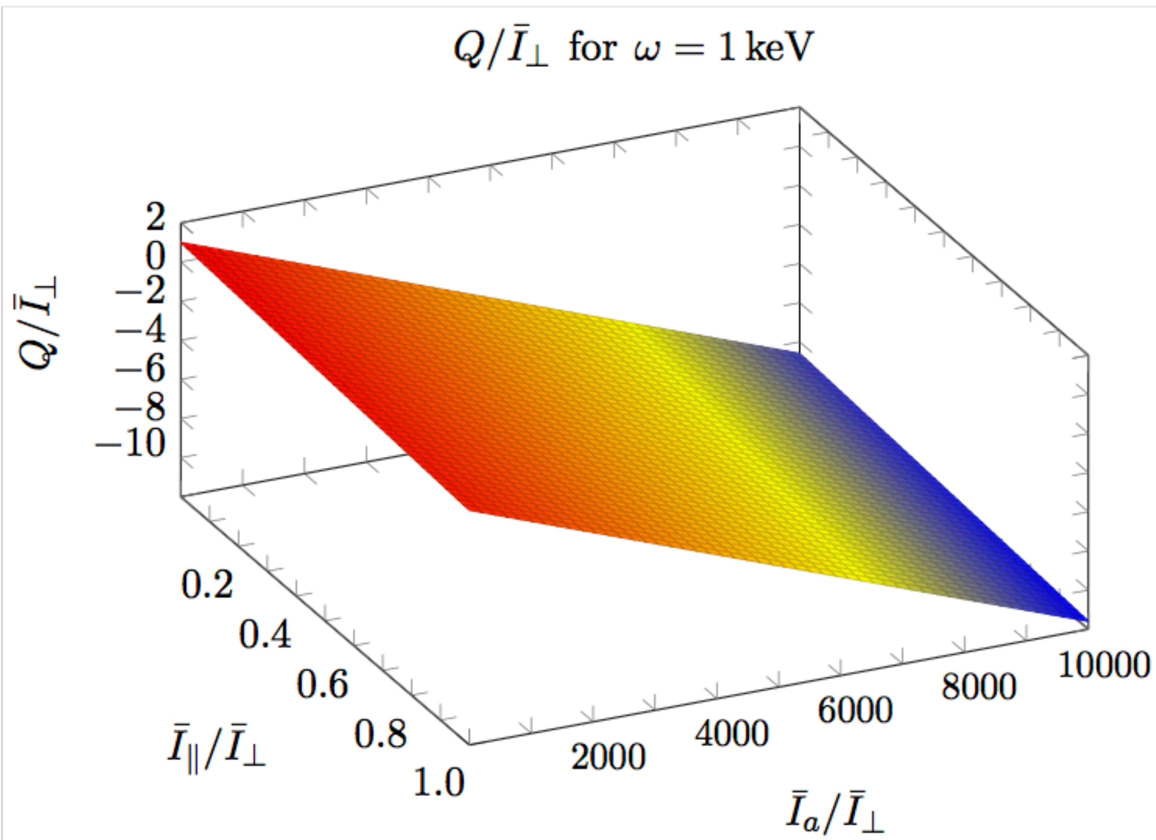

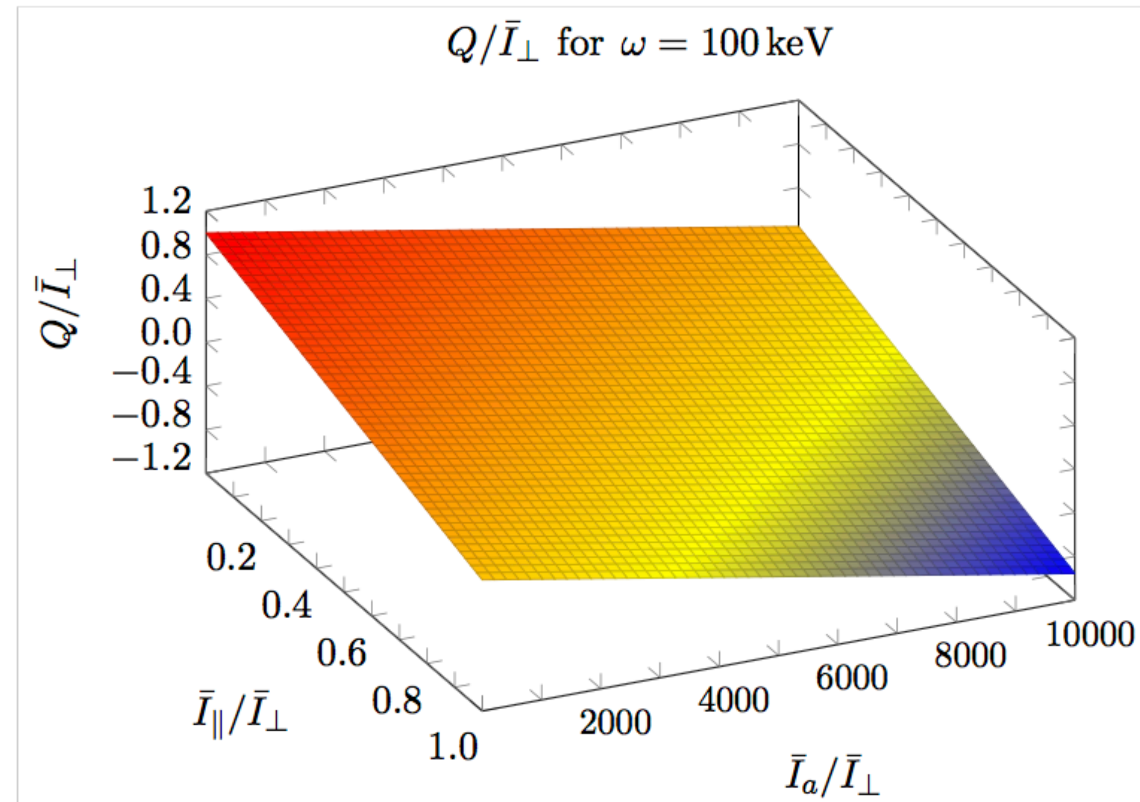

Fig. 3: (Normalized) Stokes parameter $Q/\bar{I}_\perp$ at infinity for the benchmark point $m_a = 10^{-8}\,\mathrm{keV}$, $g = 5 \times 10^{-17}\,\mathrm{keV}^{-1}$, $r_0 = 10\,\mathrm{km}$, $B_0 = 20 \times 10^{14}\,\mathrm{G}$ and $\theta = \pi/2$ in the plane $(\bar{I}_\parallel/\bar{I}_\perp, \bar{I}_a/\bar{I}_\perp)$ at the surface. The left panel corresponds to ALP energy $\omega = 1\,\mathrm{keV}$ $(P_{a\to\gamma} \approx 1.2 \times 10^{-3})$ while the right panel corresponds to $\omega = 100\,\mathrm{keV}$ $(P_{a\to\gamma} \approx 9.6 \times 10^{-5})$.

Radius of Conversion

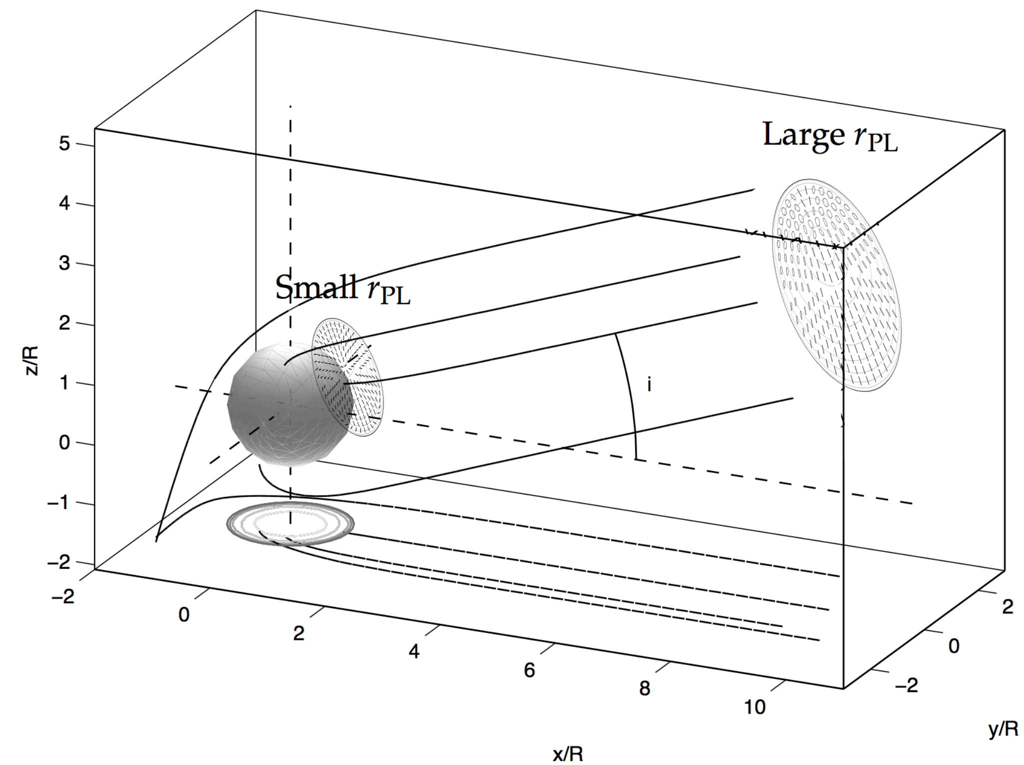

$$r_{a\to\gamma} = \left(\frac{7\alpha}{45\pi}\right)^{1/6}\left(\frac{\omega}{m_a}\frac{B_0}{B_c}|\sin\theta|\right)^{1/3} r_0$$

$$\sim 1626.9\left(\frac{\omega}{1\,\mathrm{keV}}\right)^{1/3}\left(\frac{B_0}{10^{14}\,\mathrm{G}}\right)^{1/3}\left(\frac{10^{-8}\,\mathrm{keV}}{m_a}\right)^{1/3}\left(\frac{r_0}{10\,\mathrm{km}}\right)\,\mathrm{km}.$$

$$\boxed{\frac{r_{PL}}{r_{a\to\gamma}} \sim 0.57\left(\frac{1\,\mathrm{keV}}{\omega}\right)^{2/15}\left(\frac{B_0}{10^{14}\,\mathrm{G}}\right)^{1/15}\left(\frac{m_a}{10^{-8}\,\mathrm{keV}}\right)^{1/3}\left(\frac{r_0}{10\,\mathrm{km}}\right)^{1/5}}$$

Future

Exciting time
for
ALP searches!

generally, I expect the interface between X-ray astronomy and axion physics to be a fruitful area in the future

Future

polarization signals in hard X-rays

Fortin, KS, (arXiv:1807.10773)

generalized initial states

spectral analysis

populations of magnetars?

other signals?

generally, I expect the interface between X-ray astronomy and axion physics to be a fruitful area in the future

Plasma Effects

$$i\frac{d}{dz}\Phi = \begin{pmatrix} \omega + \Delta_a & \Delta_M & 0 \\ \Delta_M & \omega + \Delta_\| + \Delta_p & \sigma_{12}\omega/2 \\ 0 & \sigma_{21}\omega/2 & \omega + \sigma_{22}\omega/2 \end{pmatrix}\Phi, \qquad \Phi = \begin{pmatrix} a \\ E_\| \\ E_\perp \end{pmatrix}$$

$$\Delta_p \approx -\omega_{\rm pl}^2/2\omega \approx -2\times 10^{-14}\ \mathrm{eV}$$

$$\omega_{\rm pl}^2 = 4\pi\alpha N_e/m_e$$

$$N_e = (7\times 10^{-2}\ \mathrm{cm}^{-3})[B_z/(1\ \mathrm{G})][(1\ \mathrm{sec})/P]$$

$$\sigma_{11} = (q - v_e)\sin^2\theta - \frac{v_e}{1-u_e}\cos^2\theta,$$

$$\sigma_{22} = -m\sin^2\theta - \frac{v_e}{1-u_e},$$

$$\sigma_{12} = -\sigma_{21} = i\frac{v_e u_e^{1/2}}{1-u_e}\cos\theta.$$

$$\Delta_p r_0 \approx \text{-}10$$

$$\Delta_{\|0} r_0 \approx 8.6\times 10^{13}$$

plasma important at $\Delta_p \approx \Delta_\|$

$$\gamma_{\rm res} = \frac{4\Delta_M^2 H}{\Delta_\|} = 1.915\times 10^{-8}\,\frac{g_9^2 H_1}{\omega_1 \hat{q}}$$

Hard X-Ray Telescope

HXMT (20-250 keV) - 2018

Hard X-ray Modulation Telescope

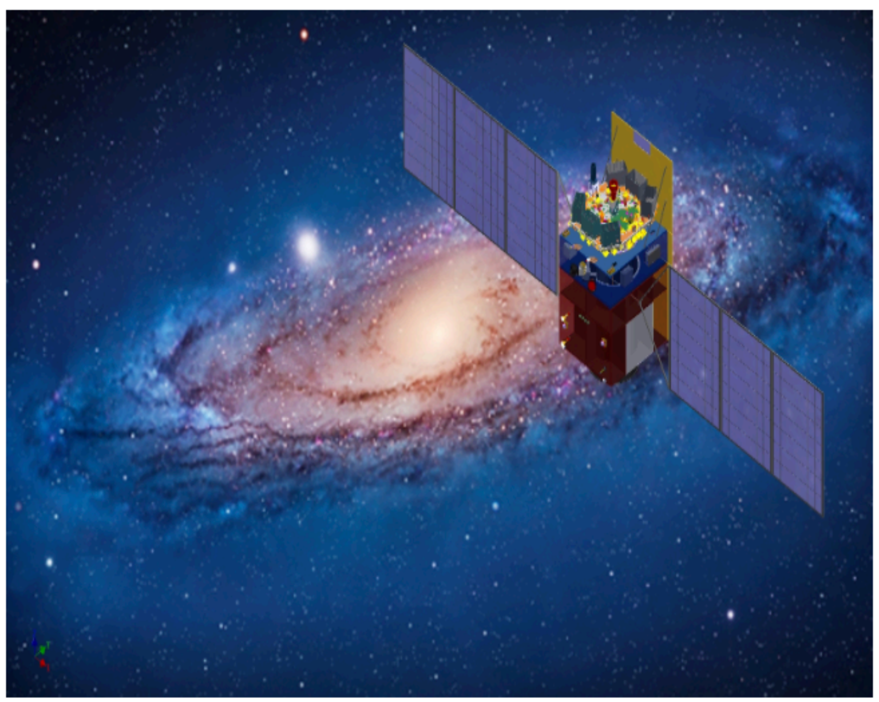

The Hard X-ray Modulation Telescope (HXMT) , named "Insight", is China's first X-ray astronomy satellite. There are three main payloads onboard Insight-HXMT, the high energy X-ray telescope (20-250 keV, 5100 cm^2), the medium energy X-ray telescope (5-30 keV, 952 cm^2), and the low energy X-ray telescope (1-15 keV, 384 cm^2). The main scientific objectives of Insight-HXMT are: (1) to scan the Galactic Plane to find new transient sources and to monitor the known variable sources, (2) to observe X-ray binaries to study the dynamics and emission mechanism in strong gravitational or magnetic fields, and (3) to find and study gamma-ray bursts with its anti-coincidence CsI detectors.

Urca Processes

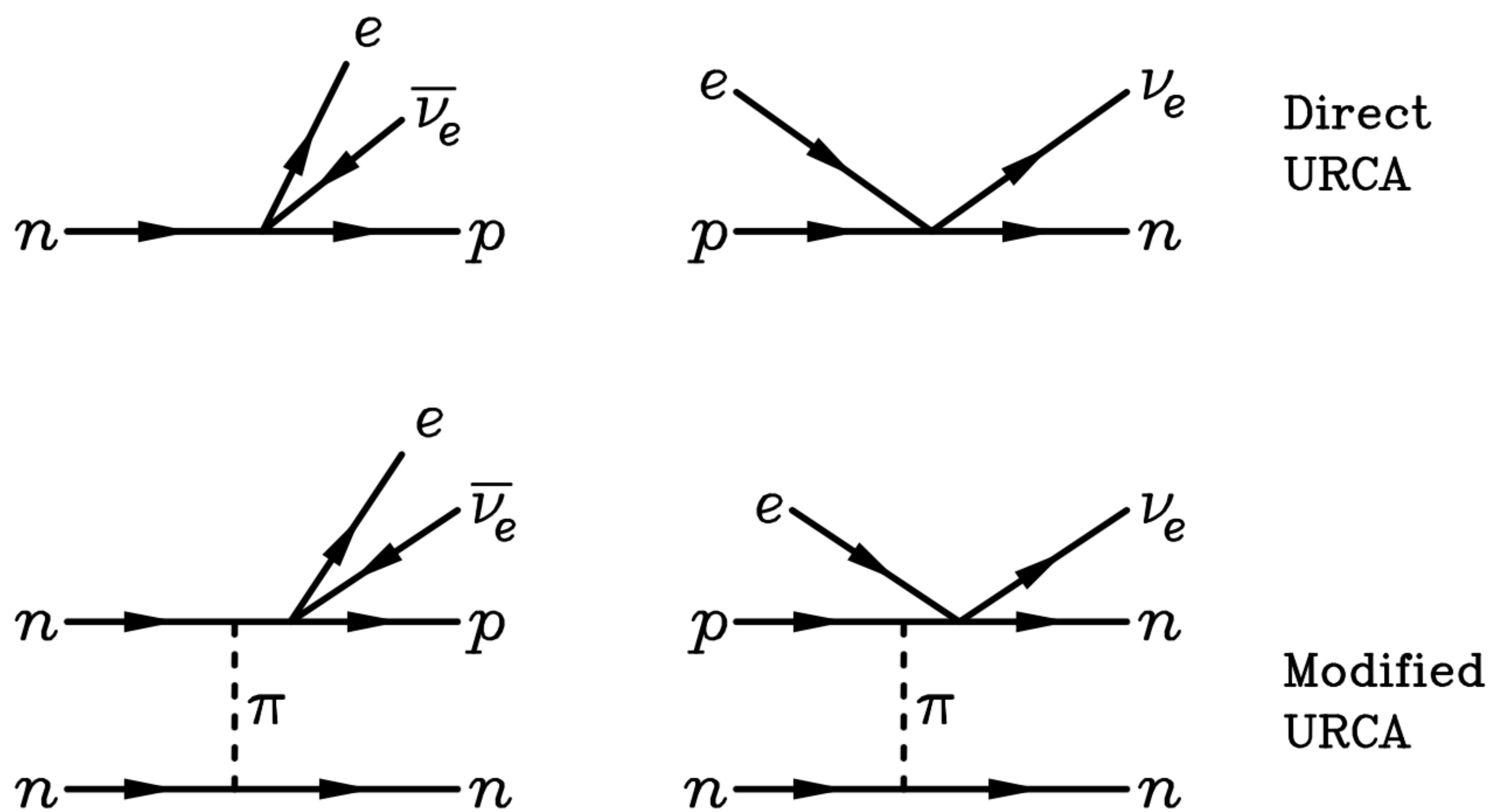

Neutrino Production

$$\dot{q}_\nu^D \sim 10^{27}\, T_9^6\, \mathcal{R}_D \,\mathrm{erg\ s^{-1}\ cm^{-3}}\ (\rho \gtrsim 10^{15}\ \mathrm{g\ cm^{-3}})$$

$$\dot{q}_\nu^M \sim 7 \times 10^{20}\, T_9^8 \left(\frac{\rho}{\rho_{\rm nuc}}\right)^{2/3} \mathcal{R}_M \,\mathrm{erg\ s^{-1}\ cm^{-3}},$$

$$\dot{q}_\nu^{CP} \sim 10^{21} \left(\frac{\rho}{\rho_{\rm nuc}}\right)^{1/3} T_9^7\, f\left(\frac{T_{\rm core}}{T_{\rm crit}}\right) \mathrm{erg\ s^{-1}\ cm^{-3}},$$

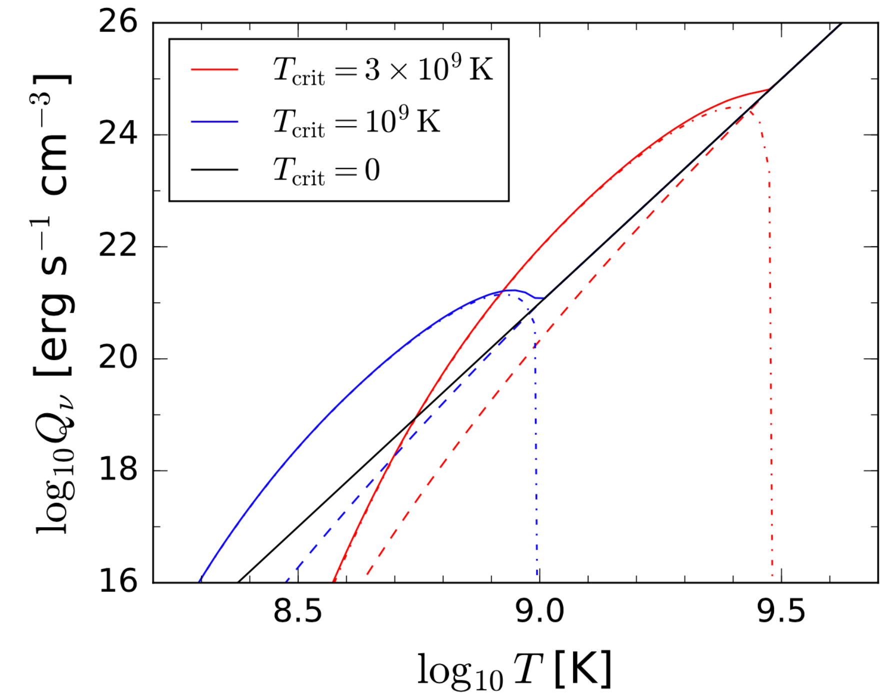

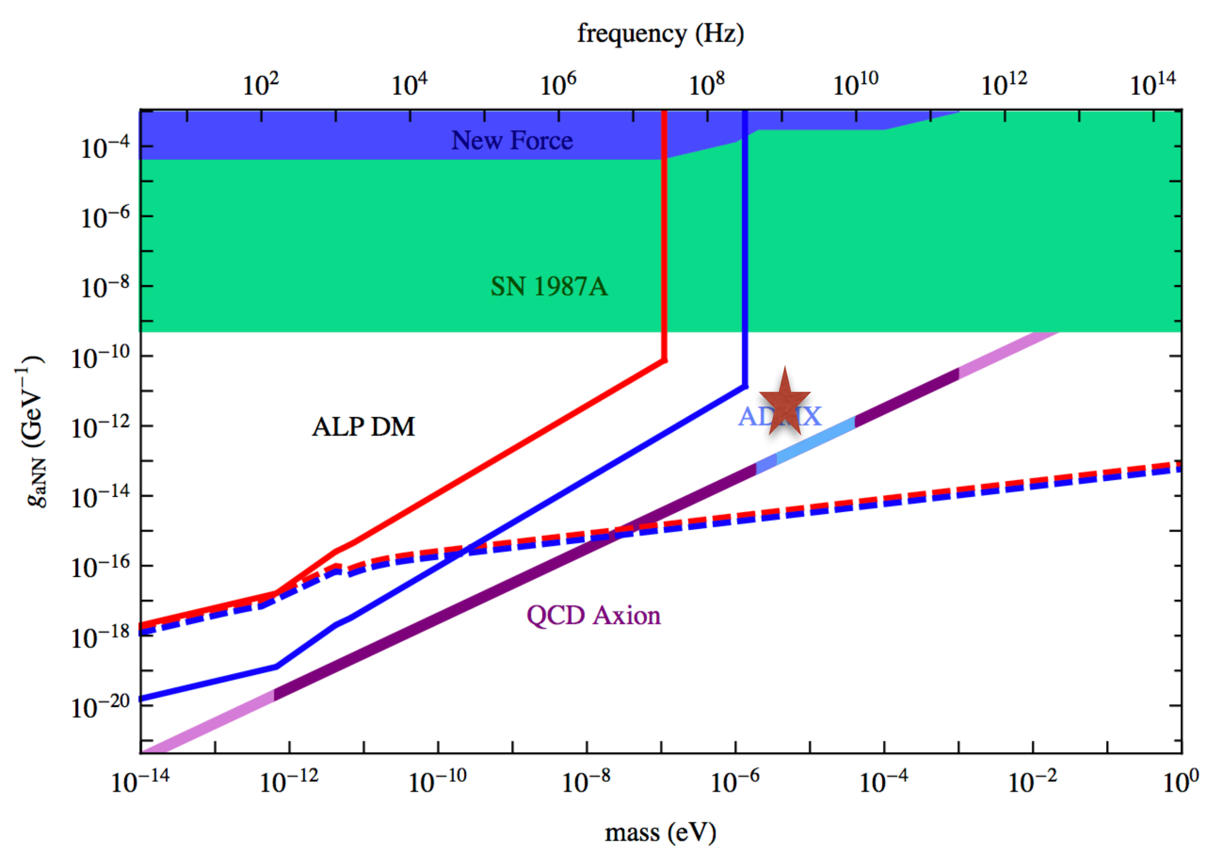

Graham et. al. (2017)

Initial Conditions

Since the focus is on the conversion probability and only the relative phase $\Delta\phi(x) = \phi_a(x) - \phi_E(x)$ appears in the equations above, one gets to

$$\begin{aligned} \frac{d\chi(x)}{dx} &= -D(x)\cos[\Delta\phi(x)], \\ \frac{d\Delta\phi(x)}{dx} &= A(x) - B(x) + 2D(x)\cot[2\chi(x)]\sin[\Delta\phi(x)], \end{aligned} \tag{2.9}$$

where $\chi(1)$ determines the initial state at the surface of the magnetar. To avoid singularities for $\chi(1) = n\pi/2$ with $n \in \mathbb{Z}$, *i.e.* for pure initial states, the initial condition for $\Delta\phi(1)$ must satisfy $\Delta\phi(1) = m\pi$ with $m \in \mathbb{Z}$. It is therefore possible to set $\Delta\phi(1) = 0$ for a pure ALP initial state[4] and the ALP-photon conversion probability is simply $P_{a\to\gamma}(x) = \sin^2[\chi(x)]$.

Magnetar Spectra

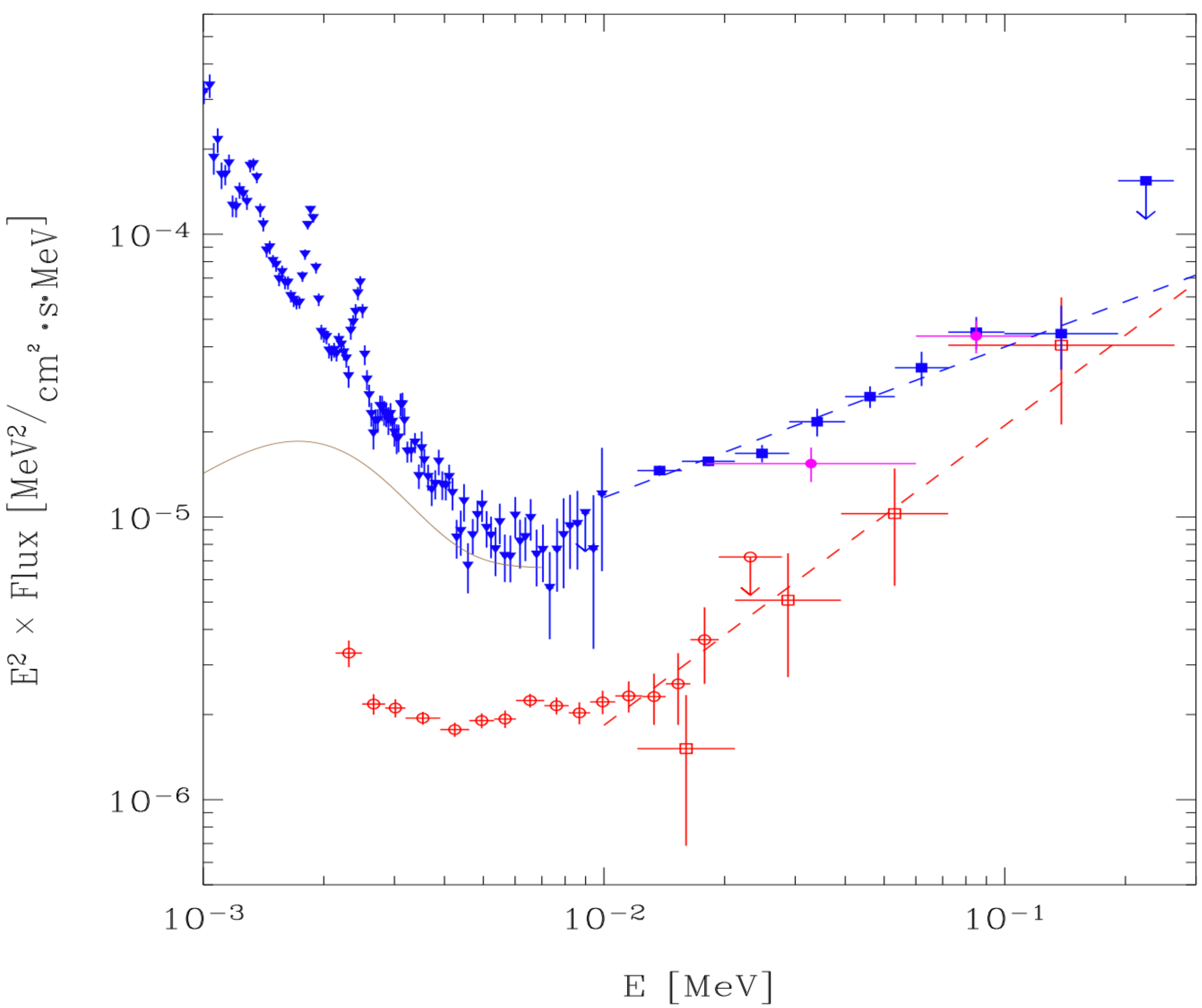

Fig. 5.— A νF_ν spectral representation of the total pulsed high-energy emission from 1E 1841-045 is shown in red (RXTE PCA; open circles, RXTE HEXTE; open squares). The total spectrum from the Kes73/1E 1841-045 complex is represented in blue (triangles; XMM EPIC PN, filled squares; RXTE HEXTE). The total (pulsed plus DC) 1-7 keV X-ray spectrum from 1E 1841-045 (Morii et al. 2003) is plotted as a solid dark orange line. The two magenta flux points are INTEGRAL IBIS ISGRI measurements given in Molkov et al. (2004). Fits (> 10 keV) to the total complex (blue) and total pulsed (red) spectra of 1E 1841-045 are drawn as dashed lines.

Kuiper et. al. (2004)

Besides spectacular outbursts, magnetars produce persistent or decaying X-ray emission with luminosity $L \sim 10^{34} - 10^{36}$ erg s^{-1}. Two peaks are observed in their X-ray spectra, with comparable luminosities. The first peak is near 1 keV; it is associated with thermal emission from the neutron star surface. The second peak is above 100 keV. Its low-energy slope (between 10 and 100 keV) was observed in 7 magnetars[1] (Kuiper et al. 2008; Enoto et al. 2010), with a typical photon index $\Gamma \sim 1 - 1.5$.

Beloborodov (2012)

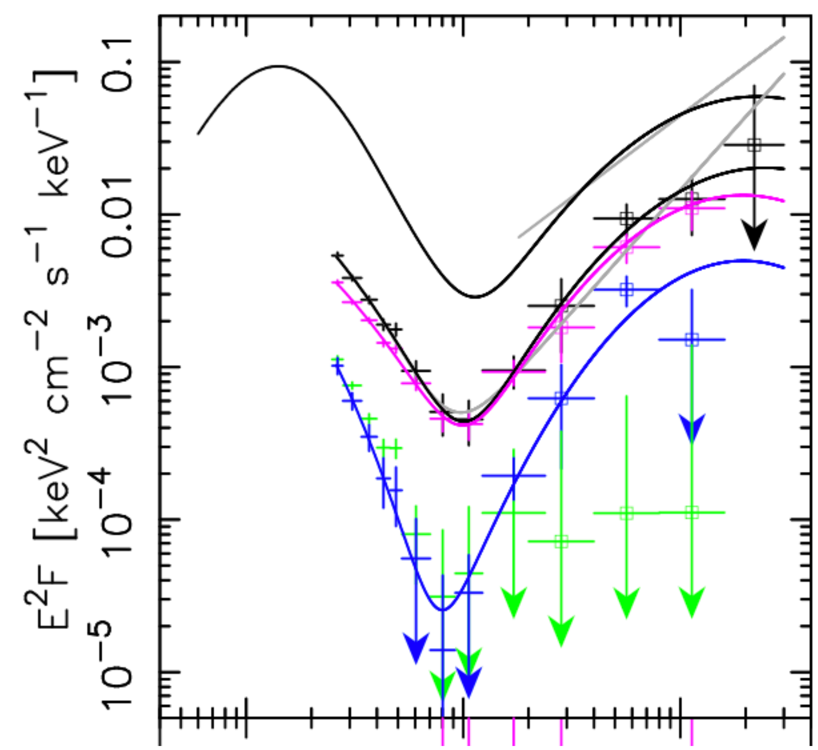

Detailed high-energy characteristics of AXP 4U 0142+61

Multi-year observations with INTEGRAL, RXTE, XMM-*Newton* and ASCA

Harotg et. al. (2008)

Axion Emissivity (pair breaking)

Keller/Sedrakian (2012)

$$\mathscr{L}_{int} = \frac{1}{f_a} B^\mu L_\mu \qquad B^\mu = C_a \bar{\psi}\gamma^\mu \gamma_5 \psi, \qquad L_\mu = \partial_\mu \phi \qquad |\mathcal{M}_a|^2 = \frac{1}{2} f_a^{-2} (B^\mu B^{\nu\dagger})(L_\mu L_\nu^\dagger)$$

The energy radiated per unit time in axions (axion emissivity) is given by the phase-space integral over the probability of the process of emission

$$\epsilon_a = -f_a^{-2} \int \frac{d^3 q}{(2\pi)^3 2\omega} \, \omega g(\omega) q_\mu q_\nu \mathrm{Im}\Pi_a^{\mu\nu}(q), \tag{7}$$

where q and ω are the axion momentum and energy. Here we defined the polarization tensor of baryonic matter

$$\mathrm{Im}\Pi^{\mu\nu}(\omega, \vec{q}) = \frac{1}{2} \sum_n (B_\mu B_\nu^\dagger) \delta^4(q - \sum_i p_i), \tag{8}$$

where the i sum is over the four-momenta of the baryons. Upon carrying out the angular integral in Eq. (7) we write the emissivity in terms of a one-dimensional integral

$$\epsilon_a = -\frac{f_a^{-2}}{4\pi^2} \int_0^\infty d|\vec{q}| \; \vec{q}^2 g(\omega) \kappa_a(q), \tag{9}$$

where the contraction of the axion currents with the baryonic polarization tensor is given by

$$\kappa_a(q) = q_\mu q_\nu \mathrm{Im}\Pi_a^{\mu\nu}(q). \tag{10}$$

Axion Emissivity (pair breaking)

$$\epsilon_a = \frac{8}{3\pi} f_a^{-2}\,\nu(0)\, v_F^2\, T^5\, I_a, \qquad I_a = z^5 \int_1^{\infty} dy\, \frac{y^3}{\sqrt{y^2-1}} f_F(zy)^2 ,$$

$z = \Delta(T)/T$ and $f_F(x) = [1+\exp(x)]^{-1}$ is the Fermi distribution function. The T^5 scaling of the emissivity is understood as follows. The integration over the phase space of neutrons carries a power of T, since for degenerate neutrons the phase-space integrals are confined to a narrow strip around the Fermi surface of thickness T. The axion is emitted thermally and being relativistic contributes a factor T^3 to the emissivity. The one power of T from the energy of the axion and the inverse one power of T from the energy conserving delta function cancel. The transition matrix element is proportional to the combinations of u_p and v_p amplitudes, which are dimensionless, but contain *implicit* temperature dependence due to the temperature dependence of the gap function. This dependence is not manifest in Eq. (22), *i.e.*, was absorbed in the definition of the integral I_a. Thus, the explicit temperature dependence of the axion emission rate Eq. (22) is T^5. In the cgs units the axion emissivity Eq. (22) is

$$\epsilon_a = 1.06 \times 10^{21} \left(\frac{10^{10}\mathrm{GeV}}{f_a}\right)^2 \left(\frac{m^*}{m}\right)^2 \left(\frac{v_F}{c}\right)^3 \left(\frac{T}{10^9\mathrm{K}}\right)^5 I_a\, \mathrm{erg\ cm^{-3}\ s^{-1}}, \qquad (24)$$

Comparing Neutrino and Axion Emissivity

Keller/Sedrakian (2012)

where two powers of v_F/c arise from the small momentum transfer expansion and one power - from the density of states. At temperatures of order the critical temperature $T_c \simeq 10^9$ K the superfluid cools primarily by emission of neutrinos via the pair-breaking processes driven by the axial-vector currents (we continue to assume that potential fast cooling via direct Urca processes is prohibited). The emissivity of this processes in the case of $^1S_0$-wave superfluid is given by [19, 20, 23]

$$\epsilon_\nu = \frac{4G_F^2 g_A^2}{15\pi^3}\zeta_A \nu(0) v_F{}^2 T^7 I_\nu, \tag{25}$$

where G_F is the weak Fermi coupling constant, $g_A = 1.25$ is the axial-vector current coupling constant, $\zeta_A = 6/7$ and

$$I_\nu = z^7 \int_1^\infty dy \frac{y^5}{\sqrt{y^2-1}} f_F\left(zy\right)^2. \tag{26}$$

We now require that the axion luminosity does not exceed the neutrino luminosity, *i.e.*,

$$\frac{\epsilon_a}{\epsilon_\nu} = \frac{10\pi^2}{f_a^2 G_F^2 g_A^2 \zeta_A}\frac{I_a}{I_\nu} < 1. \tag{27}$$

Comparing Neutrino and Axion Emissivity

Keller/Sedrakian (2012)

Substituting the the free-space value of the axial vector coupling $g_A = 1.25$ and introducing $r(z) \equiv z^2(I_a/I_\nu)$ we transform Eq. (27)

$$\frac{\epsilon_a}{\epsilon_\nu} = \frac{59.2}{f_a^2 G_F^2 \Delta(T)^2}\, r(z). \tag{28}$$

Not far from the critical temperature $\Delta(T) \simeq 3.06 T_c\sqrt{1 - T/T_c}$, which translates into $z = 3.06\, t^{-1}\sqrt{1-t}$, where $t = T/T_c$. Numerical evaluations of the integrals provides the following values $r(0.5) = 0.07$, $r(1) = 0.26$, $r(2) = 0.6$ and asymptotically $r(z) \to 1$ for $z \gg 1$. Substituting the value of the Fermi coupling constant $G_F = 1.166 \times 10^{-5}$ GeV^{-2} in Eq. (28) and noting that $r(z) \leq 1$, we finally obtain

$$f_a > 5.92 \times 10^9\,\mathrm{GeV}\left[\frac{0.1\ \mathrm{MeV}}{\Delta(T)}\right] \tag{29}$$

Light Species

There's a lot of interest in light BSM particles these days

Light Species

UV models: ALPs/dark photons in string theory

Probes at the LHC/HL-LHC etc.

Probes using atomic/molecular physics

Direct detection techniques: interferometers, light shining through wall, haloscope, etc.

Cosmological/astrophysical probes

Lots of new experimental ideas/proposals!

Why Axions?

Neutron EDM

Historically, the strong CP problem motivated axions

The classical version is visually intuitive:

credit: Hook (Brookhaven 2018)

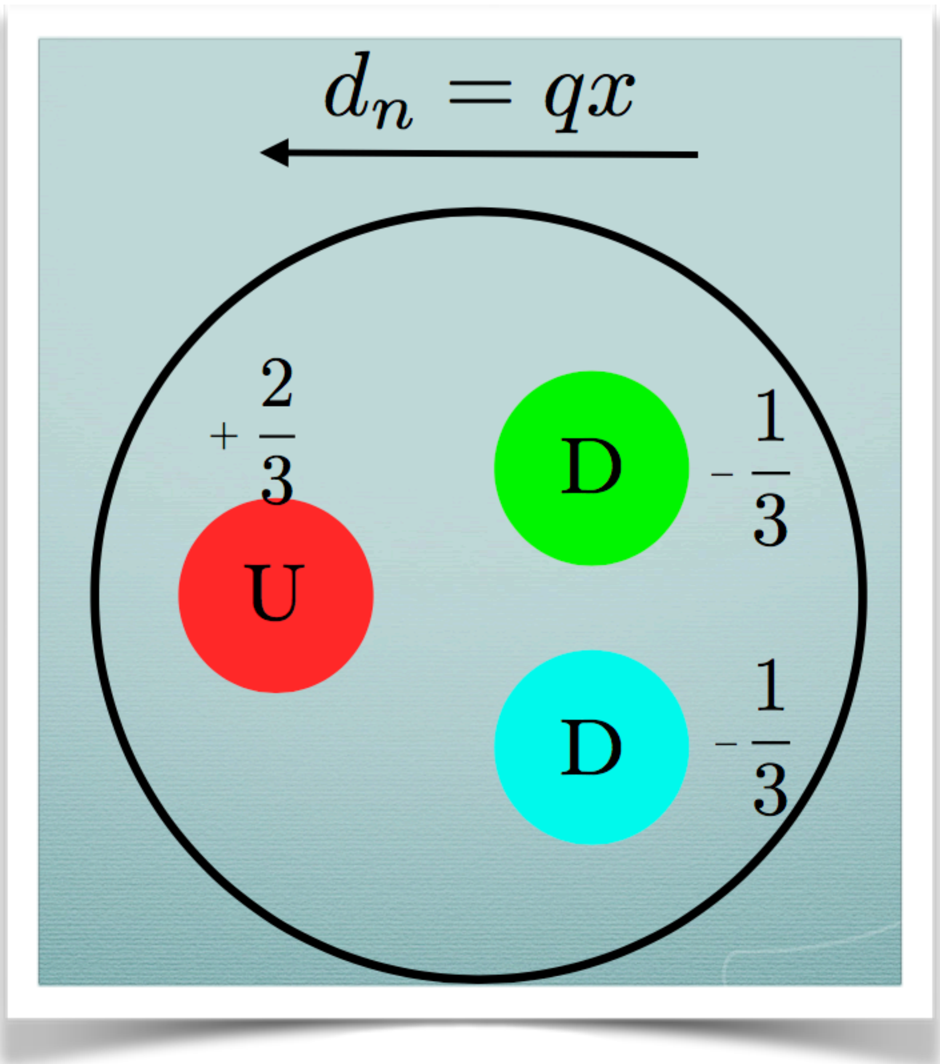

electric dipole moment of the neutron

measured to be tiny!

$$d_n < 2.9 \times 10^{-26} \text{ e cm}$$

hep-ex/0602020

How about the theory calculation?

An Unnaturally Small Angle

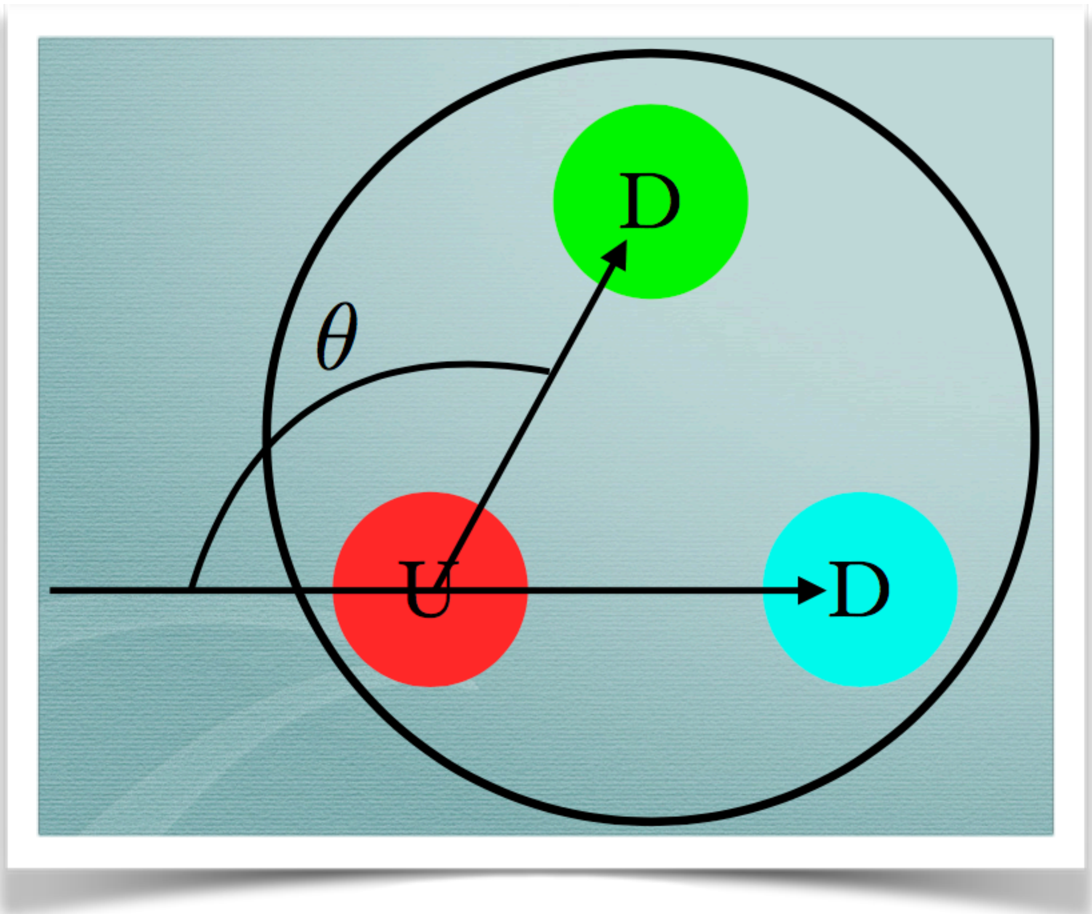

$$|d_n| \sim ex\sqrt{1-\cos\theta}$$

$$\sim 10^{-14} e\sqrt{1-\cos\theta}\ \text{cm}$$

$$\Rightarrow\ \theta\ <\ 10^{-12}\ !!$$

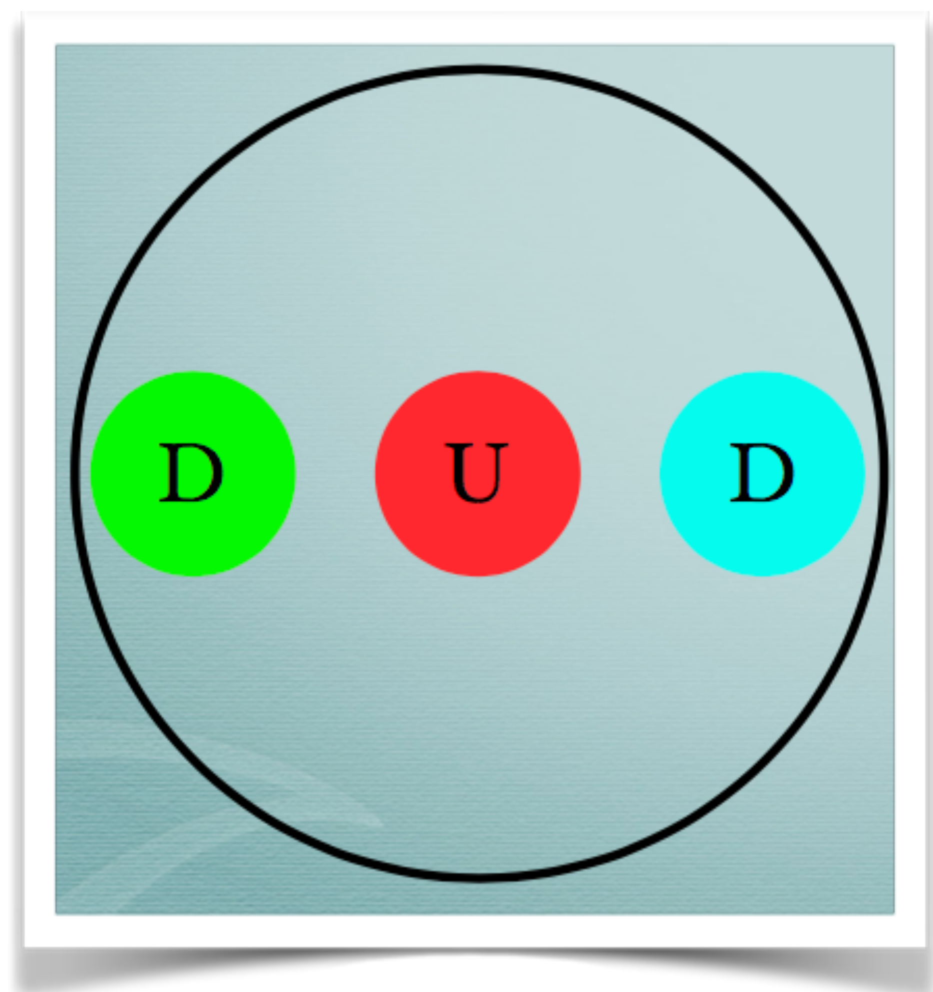

As far as we know, no “anthropic” reason

Kaloper et. al. (2017)

An example of fine-tuning

A Dynamical Angle

In chemistry, a similar question is resolved by making the angle itself dynamical

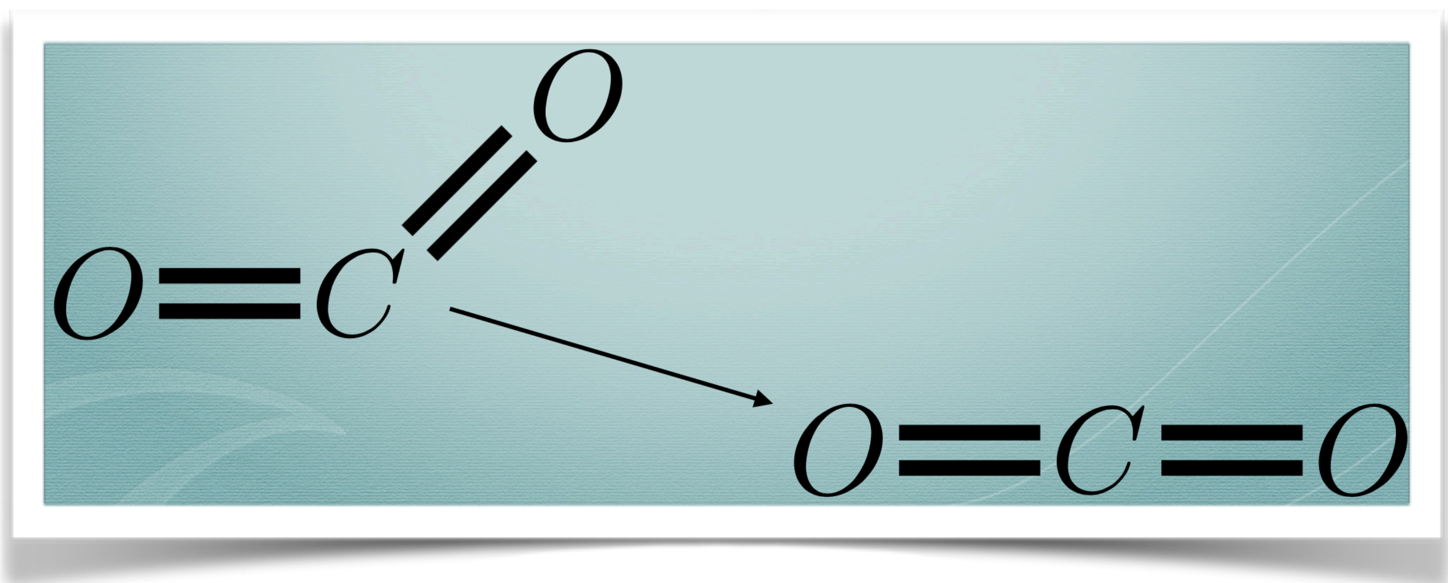

Axions are the dynamical degree of freedom

A Dynamical Angle

$$\theta\, G_{\mu\nu}\tilde{G}^{\mu\nu} \quad \Rightarrow \quad \frac{a}{f}\, G_{\mu\nu}\tilde{G}^{\mu\nu}$$

$\boxed{\text{Axions are the dynamical degree of freedom}}$

The Axiverse

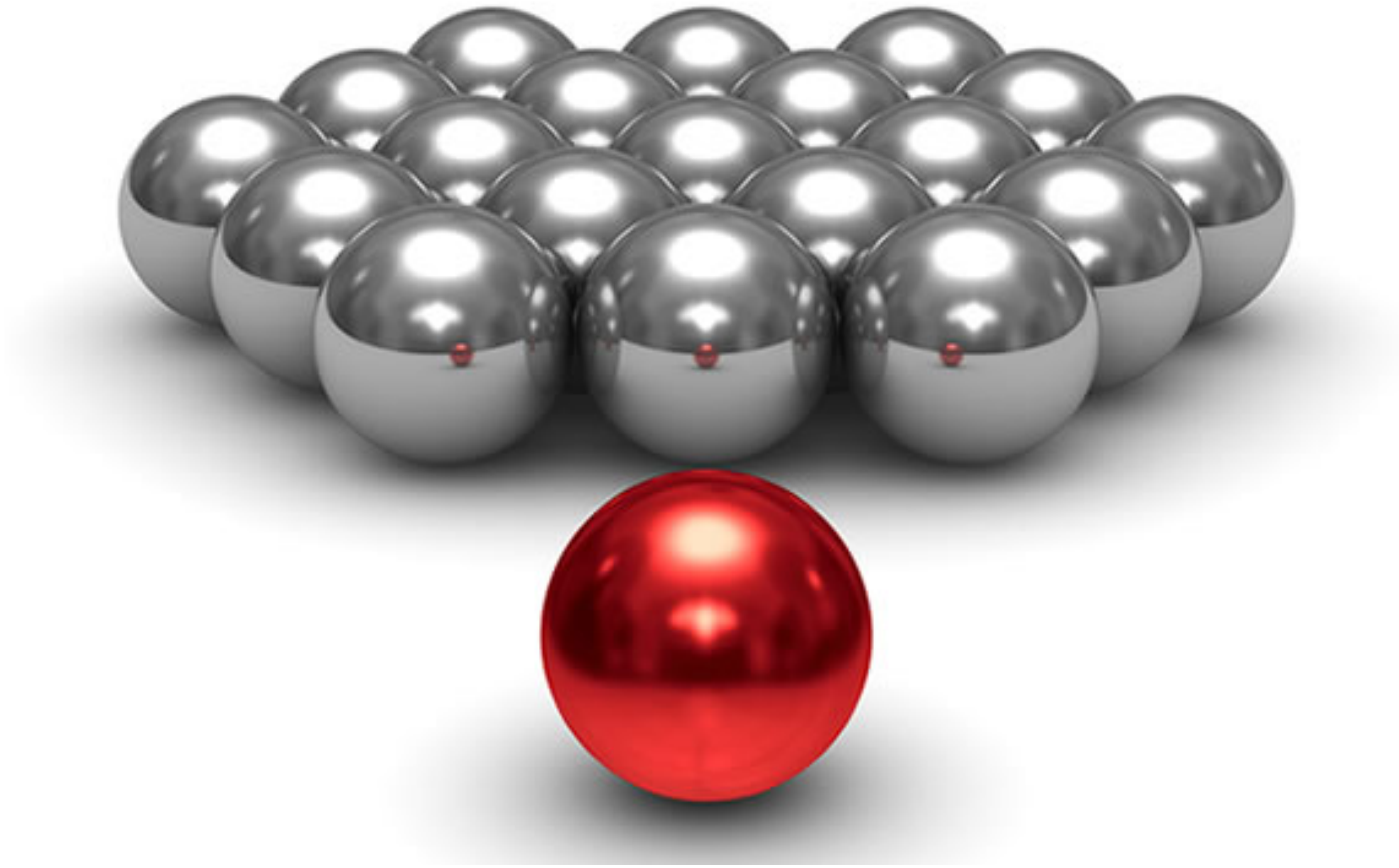

String Theory

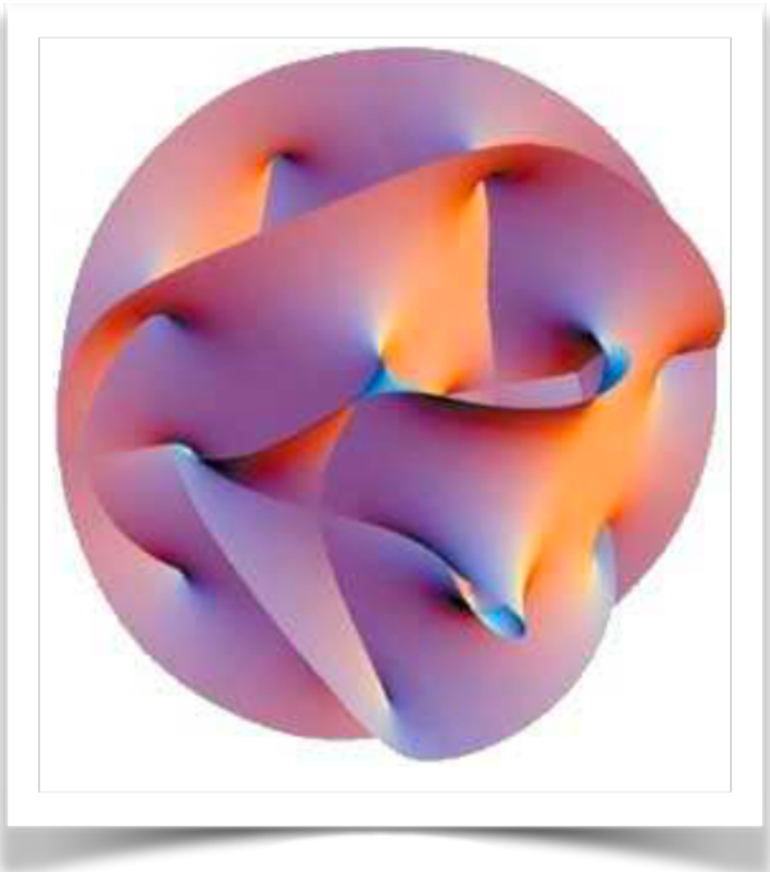

The most important prediction of string theory is the existence of extra dimensions

These extra dimensions are compactified

What are the generic features?

- Extra scalar fields: Moduli (gravitationally coupled)

$\boxed{\text{- Hundreds of pseudoscalar fields: Axion-like Particles (ALPs)}}$

String Axiverse

> Although it has been argued that there is no exact global symmetry in string theory, there can be a bunch of well-controlled approximate shift symmetries for light axions.

Witten (1985)

$$\mathcal{L}_a \sim \frac{1}{2}(\partial_\mu a)^2 + \frac{c_1}{f}\partial_\mu a J^\mu - \frac{c_2}{f} a G_{\mu\nu}\tilde{G}^{\mu\nu} - \frac{c_3}{f} a F_{\mu\nu}\tilde{F}^{\mu\nu} - \frac{1}{2}m_a^2 a^2 + \ldots$$

$$\left.\begin{array}{l} m_a \\ g \sim 1/f \end{array}\right\} \boxed{\text{Free, independent parameters for us}}$$

Arvanitaki et. al. (2012)

Cicoli et. al. (2012)

axion decay constant: depends on internal CY geometry

axion mass: mechanism of PQ breaking

ALP Detection

WIMP Detection Strategies

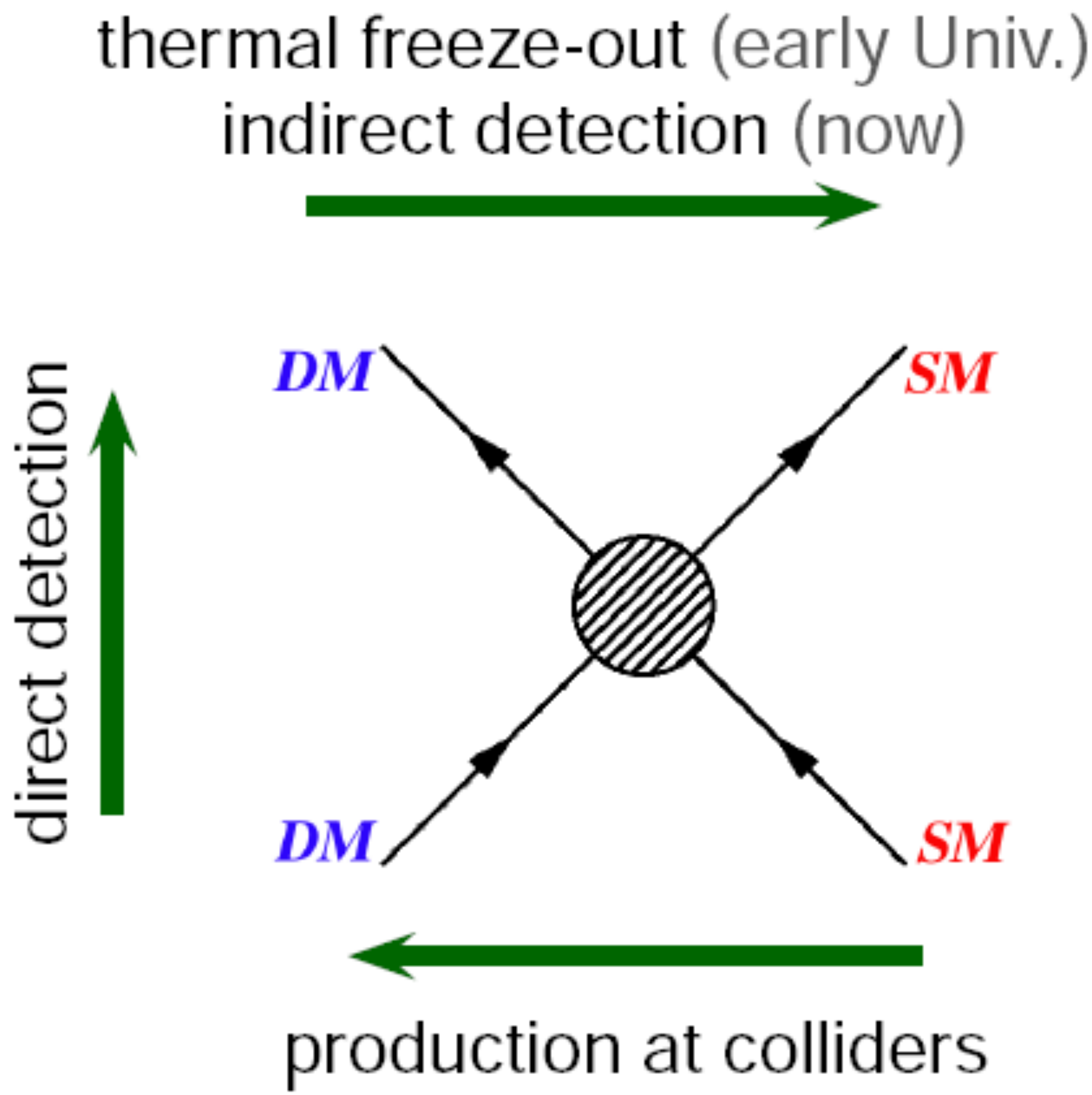

ALP Detection Strategies

emission/conversion

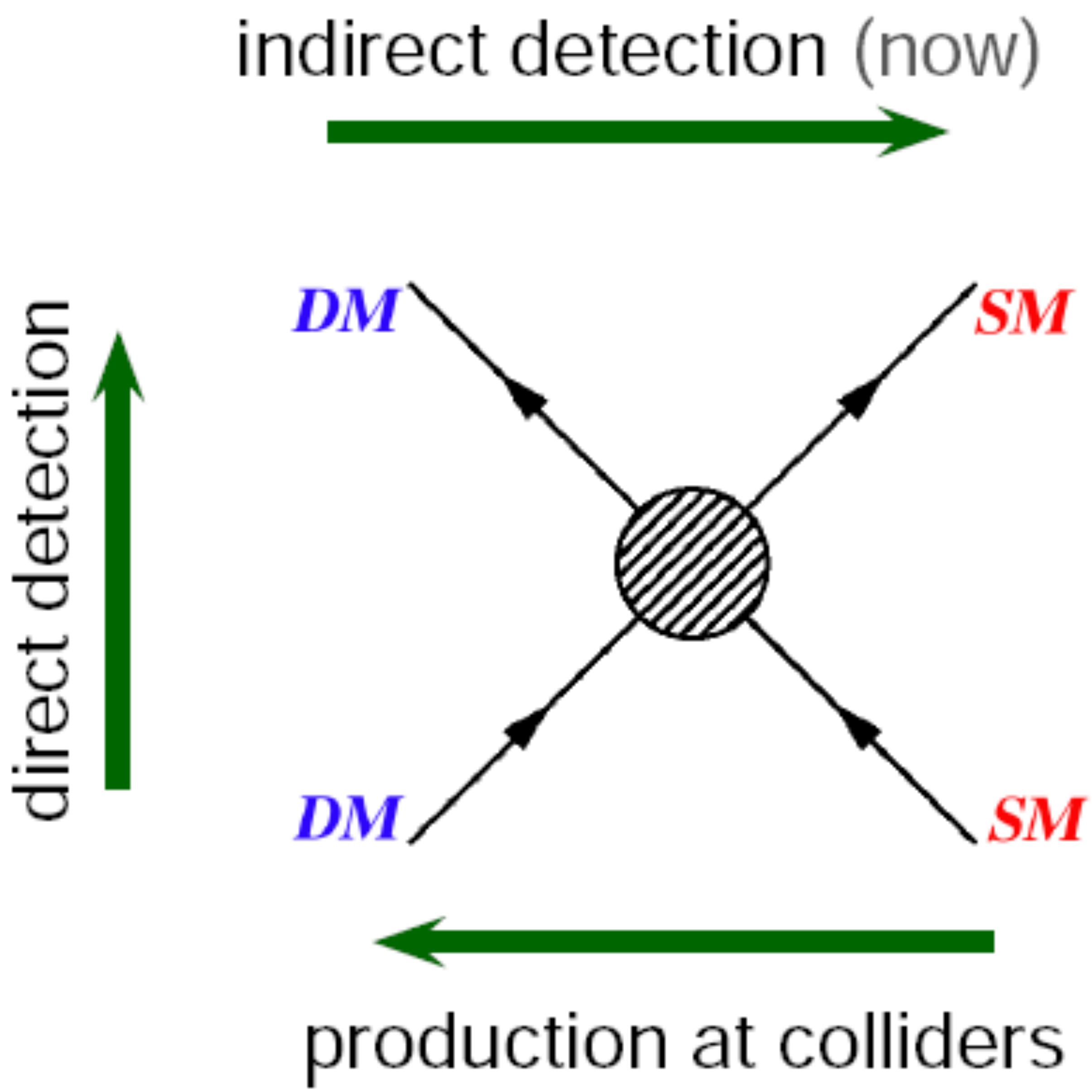

LHC/lepton collider studies

Collider Prospects

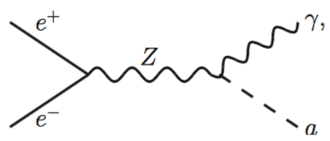

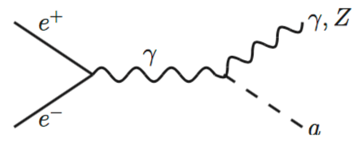

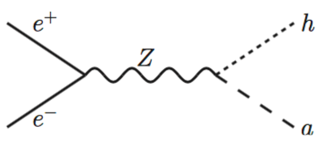

$a \to \ell^+\ell^-$

$a \to \gamma\gamma$

$Z \to \gamma a$

$a \to gg$

$$\mathcal{L}_a \sim \frac{1}{2}(\partial_\mu a)^2 - \frac{1}{2}m_a^2 a^2 + \frac{c_1}{f}\boxed{\partial_\mu a \bar{f}\gamma_\mu\gamma_5 f}$$
$$- \frac{c_2}{f}\boxed{aG_{\mu\nu}\tilde{G}^{\mu\nu}} - \frac{c_3}{f}\boxed{aF_{\mu\nu}\tilde{F}^{\mu\nu}} - \frac{c_4}{f}\boxed{aF_{\mu\nu}\tilde{Z}^{\mu\nu}} - \frac{c_5}{f}aZ_{\mu\nu}\tilde{Z}^{\mu\nu}$$
$$+ \frac{c_6}{f^2}\boxed{(\partial_\mu a)(\partial^\mu a)\phi^\dagger\phi} + \frac{c_7}{f^3}\boxed{(\partial^\mu a)(\phi^\dagger \iota D_\mu\phi} + h.c.)\phi^\dagger\phi + \ldots$$

$h \to aa$

$h \to Za$

Bauer/Neubert (2018)

Lian-Tao Wang et. al. (2017)

A. Alves, KS (2017)

Collider Prospects

Bauer/Neubert (2018)

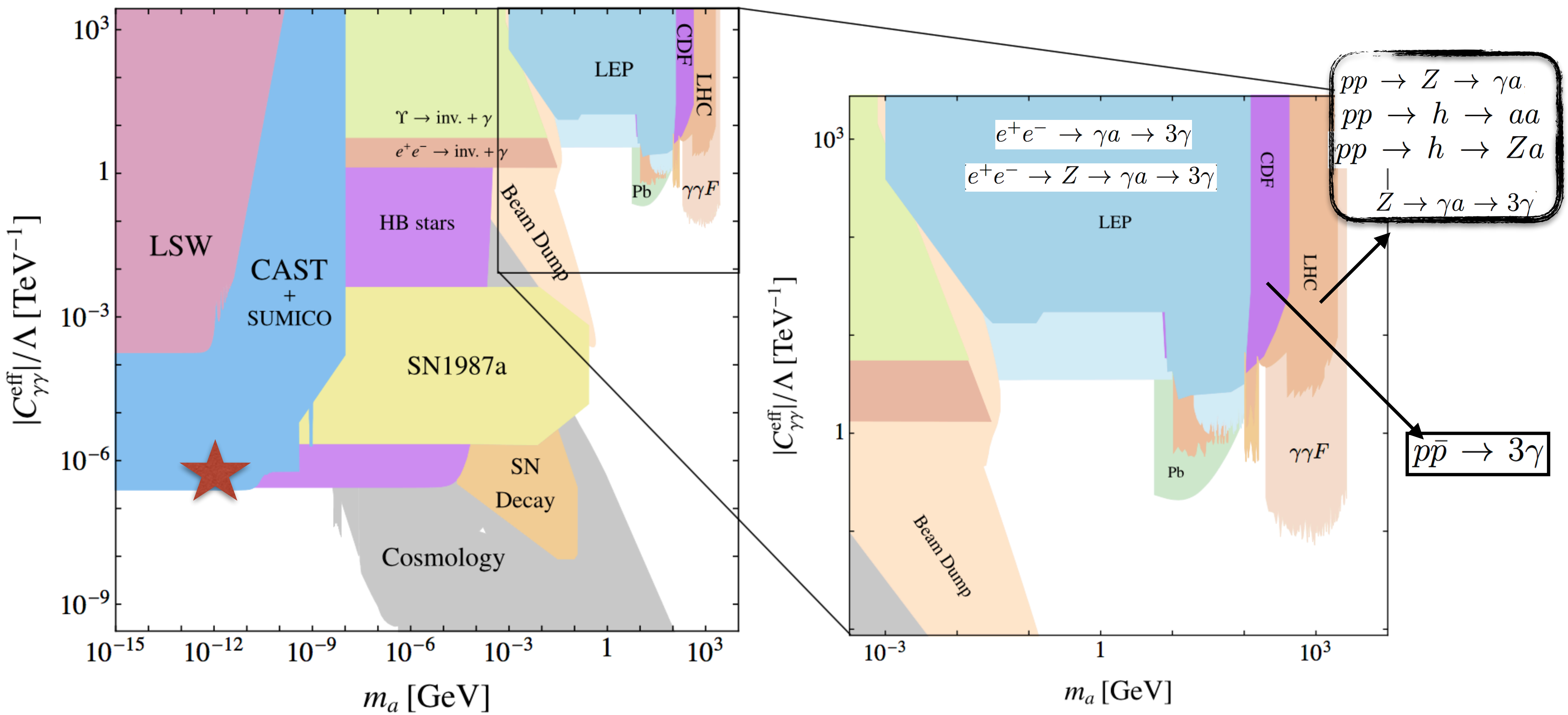

Figure 4: Left: Summary plot of constraints on the parameter space spanned by the ALP mass and ALP-photon coupling. Right: Enlarged display of the constraints from collider searches: LEP (light blue and blue), CDF (purple), LHC from associated production and Z decays (orange), LHC from photon fusion (light orange), and from heavy-ion collisions at the LHC (green).

Conversion as ALP Detection Tool

Strategy:

1. Photons/ALPs travel from A to B

2. There’s a magnetic field between A and B

3. Photon-ALP interconversion happens

4. Photon spectrum at B shows changes

Astrophysical Probes of Conversion

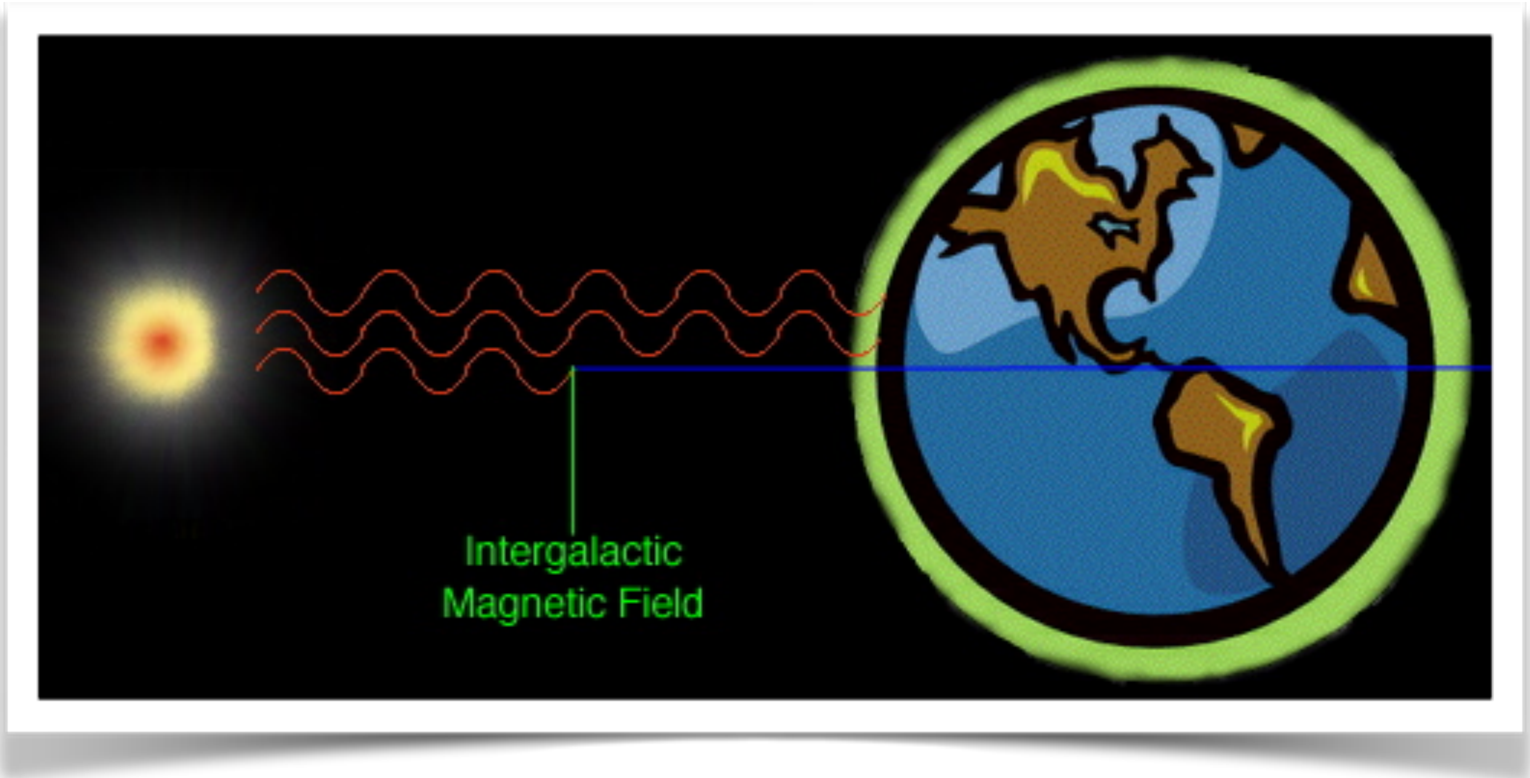

Fig.: John Terning

Conversion Probability

$$p(a \to \gamma) = \sin^2(2\theta)\ \sin^2(\pi z / L_{\mathrm{osc}})$$

mixing strength

follows directly from Maxwell's equations

Supernova dimming with ALPs

Csaki et. al. (2001)

ALPs from AGNs giving X-rays

Conlon et. al. (2014)

Constant B field, simple analytic solution

Strong QED

Strong $$B_k = \frac{m^2c^3}{e\hbar} \approx 4.4 \times 10^{13}\,\mathrm{G}$$

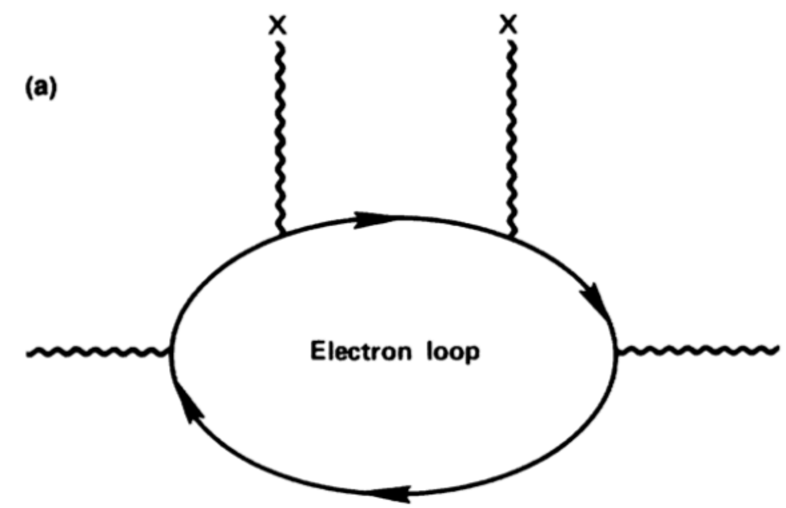

Euler-Heisenberg Lagrangian:

$$\omega < m \sim 500 \text{ keV}$$

Weak field limit:

Heyl/Hernquist (2012)

$$I = F_{\mu\nu}F^{\mu\nu} = 2\left(|\mathbf{B}|^2 - |\mathbf{E}|^2\right) \qquad K = \left(\frac{1}{2}\epsilon^{\lambda\rho\mu\nu}F_{\lambda\rho}F_{\mu\nu}\right)^2 = -(4\mathbf{E}\cdot\mathbf{B})^2$$

$$\mathcal{L} \approx -\frac{1}{4}I + E_k^2\frac{e^2}{hc}\left[\frac{1}{E_k^4}\left(\frac{1}{180}I^2 - \frac{7}{720}K\right) + \frac{1}{E_k^6}\left(\frac{13}{5040}KI - \frac{1}{630}I^3\right)\cdots\right]$$

Why Neutron Stars?

Strong magnetic fields are especially useful

Magnetars have the strongest magnetic fields

Also lots of data

Formal side:

$\boxed{\text{Non-constant magnetic field, interesting equations}}$

$\boxed{\text{Strong magnetic field, so non-linear QED effects}}$

Full QED Lagrangian

$$\mathcal{L}_0 = -\frac{1}{4} I,$$

$$\mathcal{L}_1 = \frac{e^2}{hc} \int_0^\infty e^{-\zeta} \frac{d\zeta}{\zeta^3} \left\{ i\zeta^2 \frac{\sqrt{-K}}{4} \times \frac{\cos\left(\frac{\zeta}{B_k}\sqrt{-\frac{I}{2} + i\frac{\sqrt{-K}}{2}}\right) + \cos\left(\frac{\zeta}{B_k}\sqrt{-\frac{I}{2} - i\frac{\sqrt{-K}}{2}}\right)}{\cos\left(\frac{\zeta}{B_k}\sqrt{-\frac{I}{2} + i\frac{\sqrt{-K}}{2}}\right) - \cos\left(\frac{\zeta}{B_k}\sqrt{-\frac{I}{2} - i\frac{\sqrt{-K}}{2}}\right)} + |B_k|^2 + \frac{\zeta^2}{6} I \right\}$$

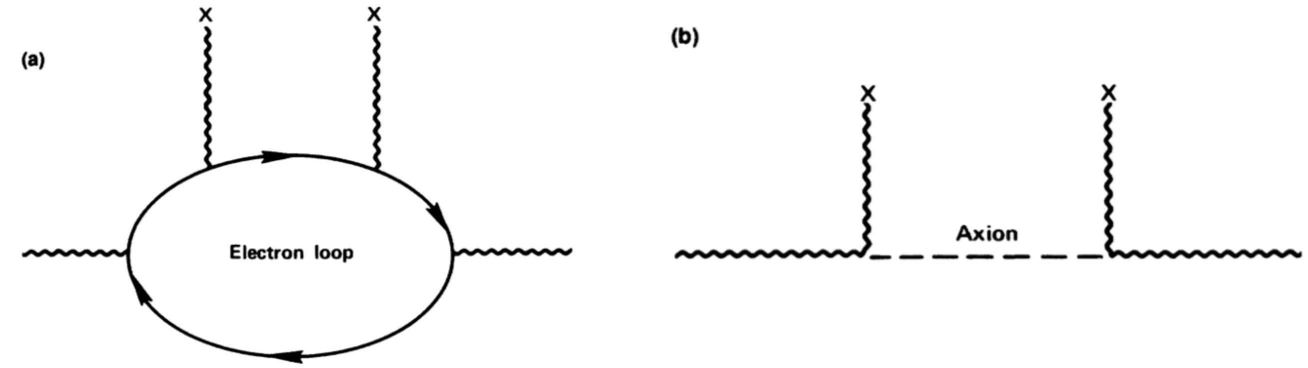

QED effects can change the spectrum from magnetars

Studied extensively by astrophysics community

Heyl, Ho, Perna, Taverna, Turolla, etc.

$$\boxed{\begin{aligned} n_\perp &= 1 + \epsilon_\perp b^2 \\ n_\parallel &= 1 + \epsilon_\parallel b^2 \end{aligned}}$$

Refractive Indices

Heyl/Hernquist (2012)

Perpendicular (X-mode)

$$n_\perp \sim 1 + \Delta_\perp/\omega \qquad \Delta_\perp = \frac{1}{2} q_\perp \omega \sin^2\theta$$

$$q_\perp = \frac{4\alpha}{45\pi} b^2 \hat{q}_\perp \qquad \hat{q}_\perp = \frac{1}{1 + 0.72 b^{5/4} + (4/15) b^2}$$

Parallel (O-mode)

$$n_\| \sim 1 + \Delta_\|/\omega \qquad \Delta_\| = \frac{1}{2} q_\| \omega \sin^2\theta$$

$$q_\| = \frac{7\alpha}{45\pi} b^2 \hat{q}_\| \qquad \hat{q}_\| = \frac{1 + 1.2b}{1 + 1.33b + 0.56b^2}$$